Characterization of Low-Rank Coal Char Used in the Production of Hydrogen

R.C. Timpe, R.E. Sears, and G.G. Montgomery

University of North Dakota Energy Research Center
Box 8213 University Station, Grand Forks, ND 58202

INTRODUCTION

The production of low-cost hydrogen for use as a fuel and chemical feedstock to supplement fossil fuels and provide a feasible alternative to current hydrogen production methods is of continued interest in the energy field. The demand for hydrogen is increasing, with the need for hydrogen predicted to rise by a factor of 15 to 20 times over the next 40+ years (1).

Presently industrial quantities of hydrogen are produced primarily by either steam reforming of natural gas or partial oxidation of petroleum. However, both of the feedstocks for these processes are used more efficiently and economically in their chemically unaltered or physically refined forms. One of the most viable alternatives for hydrogen production, in terms of available feedstock, is in the use of advanced coal gasification processes. In coal gasification processes, hydrogen is produced by the following reactions:

$$C(s) + H_2O(g) \longrightarrow CO(g) + H_2(g) \quad 1)$$
$$CO(g) + H_2O(g) \longrightarrow CO_2(g) + H_2(g) \quad 2)$$

The gasification reaction 1) involves reacting coal char and steam to produce carbon monoxide and hydrogen. Additional hydrogen is produced via the water/gas shift reaction 2). The gasification step, reaction 1), is enhanced at reaction temperature by the presence of catalysts, of which the most widely studied are alkali salts (2). The alkali carbonates, bicarbonates, oxides, and hydroxides are well known as rate enhancers, while halides of the alkalis do not function nearly as well as positive catalysts. Low-rank coal offers a plentiful and relatively inexpensive substrate from which to form char that has high reactivity (higher than those of higher-rank coals) toward steam in a char-steam reaction 1) to produce hydrogen.

The thermodynamics of the water/gas shift reaction 2) require that the hydrogen production process operate at the lowest temperature possible. The limit to which the temperature may be lowered in the process is governed by the activity of the char generated at that temperature from a particular coal. Laboratory-scale experiments have shown that the 700°-800°C range at ambient pressure provide conditions for maximum production of hydrogen in the gaseous product (3). The catalytic enhancement of the rate of hydrogen production allows the operating temperature to be lowered, thus effecting greater shift and maximizing hydrogen formation.

Potassium carbonate is probably the most extensively studied of the alkali salt catalysts and is often used as a standard for comparison of catalyst effects. Other potassium compounds (except for the halides) have been shown to be excellent catalysts for the gasification of coal chars (4,5). Sodium compounds have also been studied extensively for their effect on the gasification reaction. They too have been shown to be good catalysts and in some cases were as good as the potassium compounds (5). Trona and nahcolite, naturally occuring sodium-rich minerals, have been shown in laboratory-scale experiments to be as good as potassium carbonate for catalyzing the char-steam reaction of some low-rank coals (5).

From an economic standpoint, the sodium compounds are less expensive than potassium compounds, and mineable sodium-rich minerals are even less expensive than the pure sodium compounds. However, not all low-rank coals give the same reactivity or realize the same catalytic rate enhancement under the same reaction conditions; i.e., coal-specific effects are often evident. Therefore, thorough characterization of the chars generated at the various temperatures of interest and their response to various catalysts are important in understanding the mechanism of the gasification reaction in the production of hydrogen. The research reported here involves the characterization of chars from two low-rank raw coals, Velva (North Dakota) lignite and Martin Lake (Texas) lignite. The chars were generated in the temperature range 650°-750 °C, at atmospheric pressure under inert atmosphere. Chars were also prepared from Velva and Martin Lake lignites containing added catalyst (10 wt% K_2CO_3 and Trona) at the same conditions for characterization.

EXPERIMENTAL

The reaction between low-rank coal chars and steam to produce hydrogen was studied with two different Thermogravimetric Analysis (TGA) systems. The kinetic study of weight change of carbon with time for the char-steam reaction was carried out on a DuPont 951 Thermogravimetric Analyzer (TGA) interfaced with a DuPont 1090 ThermalAnalyzer. Approximately 20 mg samples of -100 x +140 mesh uncatalyzed or catalyzed coal were devolatized under argon flowing at 160 cc/min, and the resulting char was reacted with steam ($p_{(H_2O)}$ = 0.1). Weight, time, and temperature data were recorded, and each experiment was terminated when weight loss ceased. Total gas (product gas plus carrier gas) samples were collected over the duration of the run and were analyzed by gas chromatography (GC). Selected experiments were duplicated on a large TGA so that larger gas samples could be collected, ensuring sufficiently accurate analysis. The large TGA was built at the University of North Dakota Energy Research Center (UNDERC) using a Cahn 1000 electrobalance and a 1200°C vertical tube furnace for reacting samples >1 g. Reactivity parameters, (k), for 50% carbon conversion, were calculated at each of three temperatures (T) and Arrhenius plots of ln k vs 1/T were constructed for calculating energy of activation (Ea) and frequency factor, (A), as previously described (3). Residue remaining after the reaction was analyzed by X-Ray Diffraction and X-Ray Fluorescence techniques.

Char analyzed by spectroscopic techniques was prepared as in the char-steam reaction experiments, but was cooled to room temperature under argon. In selected experiments the char was removed from the TGA under argon and stored under argon to prevent exposure to air. These samples were analyzed by Electron Spectroscopy for Chemical Analysis (ESCA) and solid state ^{13}C Cross Polarization/Magic Angle Spinning (CP/MAS) Nuclear Magnetic Resonance Spectrometry (NMR). Catalyzed and uncatalyzed samples of char were examined by Scanning Electron Microscopy (SEM), to determine surface elemental composition and to obtain photographs of the char surface. The field was scanned and representative particles were photographed and mapped to determine elemental distribution. All char samples were analyzed for active sites by gravimetric measurement of CO_2 adsorption in a manner similar to that described by Ratcliffe and Vaughn (6).

RESULTS AND DISCUSSION

There are several significant chemical differences between the coals used in this study. The Velva lignite is a northern Great Plains lignite, whereas the Martin Lake lignite is a Gulf Coast lignite and as such reflect significantly different coal-forming environments. Proximate and ultimate analyses of the two coals are listed in Table 1. The Martin Lake sample was higher in moisture and significantly lower in ash content than the Velva sample. The moisture-free (mf) oxygen value for the Martin Lake coal is 18% lower than that for the Velva, and the C/H ratio is 1.18 for Martin Lake compared to 1.30 for Velva. The normalized

product gas compositions shown in Table 2 were determined by gas chromatography (GC) on the total gas sample collected during the hydrogen production reaction carried out on both the DuPont TGA and the large laboratory TGA. The normalized hydrogen values approximated those predicted by the engineering thermodynamic model. The values obtained from the samples generated on the large TGA have somewhat less uncertainty in analysis since the dilution effect of the carrier gas was reduced.

TABLE 1

PROXIMATE AND ULTIMATE ANALYSES

Proximate Analyses	Velva	Martin Lake
Moisture %	29.3	34.8
Ash, wt % mf	13.5	8.7
Volatile Matter, wt % mf	39.3	44.0
Fixed Carbon, wt % mf	47.2	47.4
Heating Value, Btu/lb	7185	7525
Ultimate Analyses, mf		
Hydrogen	3.84	4.71
Carbon	59.93	66.46
Nitrogen	0.94	1.18
Sulfur	0.53	0.86
Oxygen (Diff)	21.26	18.09

TABLE 2

PRODUCT GAS IN MOLE % FROM VELVA LIGNITE CHAR-STEAM REACTION - LARGE TGA

Sample*	Temp. °C	H_2	CO_2	CO	CH_4
W/10 wt% Trona	750	56.23	30.13	13.64	ND
W/10 wt% Trona	700	51.73	43.51	4.55	ND
Uncatalyzed	750	57.70	35.30	6.30	0.72
Uncatalyzed	700	56.20	40.00	2.60	0.90

ND = Absent or below detection limit

*Sample sizes were between 1.0 and 1.4 grams of -100 +140 mesh "as received" coal- catalyst.

Data normalized to exclude carrier gas and air.

The inherent mineral matter of the Velva lignite had the effect of increasing the reaction rate over that of the Martin Lake lignite. Addition of either potassium or sodium compounds also increased the rate of the char-steam reaction for both the Martin Lake and the Velva char. Potassium carbonate and Trona admixed with the lignite both gave positive catalysis of the char-steam reaction. The activity parameter (k in g/hr/g) increased from 1.40 with no catalyst to 3.50 with 10 wt% K_2CO_3 and to 3.23 with 10 wt% Trona for Velva lignite at 700°C. The reactivity parameter also increased from 0.74 with no catalyst addition to 1.41 with 10 wt% K_2CO_3 and 2.37 with 10 wt% Trona for Martin Lake lignite at 700°C.

SEM photographs (Figure 1) show the surface effect, upon charring, of adding K_2CO_3 catalyst to the coals. The ragged, irregular surface and lack of apparent pores in the uncatalyzed char is in contrast to the rounded, highly porous surface on the alkali catalyzed char. The degree to which the surface changed with the addition of catalyst differed between the Velva and the Martin Lake chars. The Velva char surface is remarkably porous and contained uniform, evenly spaced nodules of approximately 0.05 μm x 0.10 μm in size. The nodules on the surface of the catalyzed Martin Lake char were neither uniform in size nor evenly spaced over the surface. The reactivities differed similarly, with the Velva having the higher reactivity. This suggests that the increase in reactivity of the catalyzed char, which may be due to mechanistic change in the chemical reaction brought about by the alkali catalyst, must also be due, at least in part, to the physical effect of producing a large increase in surface area. The result of this increase in surface area is an increase in available active sites as shown in Figures 2 and 3 for Velva char and Martin Lake char, respectively.

SEM mapping of the surface for inorganic element distribution showed that the potassium was distributed uniformly over the surface of the Velva particles. This was not the case with the Martin Lake particles. The uniform distribution of the potassium catalyst on the surface of the Velva char implies a surface wetting by a fluid consisting of, or containing, the catalyst. The Trona, however, does not exhibit this mode of distribution. Instead the element distribution map showed the sodium surface deposits as being associated with those of silicon and aluminum. The irregularly placed surface nodules of nonuniform size were located near the sodium deposits.

Carbon 13 Nuclear Magnetic Resonance (^{13}C NMR) spectra of chars prepared at temperatures from 600° to 750°C (Figure 5) indicated the absence of aliphatic groups in the char with removal of aliphatics occurring during the charring process. Aromatic CO groups and carboxyl, amide, and ester groups are absent in the chars as well. The decrease in aromatic signal strength with temperature may result from unobserved carbon in CP/MAS due to the decrease in H/C with the char (7). Table 3 shows the ESCA surface carbon/oxygen ratio on the Velva chars prepared at various temperatures. Char prepared at 750°C and exposed to air had a significantly lower surface C/O ratio than that prepared at the same temperature and protected from exposure to air. The latter sample was analyzed at the natural surface, and then at surfaces produced by removal of outer layers of char using ion "sputtering" for the time indicated on Table 3. The low C/O ratio of the exposed sample is due to the adsorption of oxygen on exposure to air. Higher oxygen contents are related to the highly activated carbon that results during the char formation. The chars formed at the other temperatures given on Table 3 exhibited little increase in C/O ratio with temperature. These results indicate that erroneous surface data can be minimized by maintaining an inert atmosphere over the char samples and a more accurate analysis can be carried out.

TABLE 3

ESCA RESULTS--VELVA LIGNITE CHAR (ELEMENT %)

Char Temp. (°C)	Sputter Time (minutes)	Element % C	O	N	C/O
750*	0	74.4	21.0	---	4.73
750	0	82.1	14.3	---	7.69
	10	82.9	13.0	---	8.52
	70	84.3	11.6	---	9.62
700	70	81.9	10.9	0.9	10.03
650	70	80.1	12.3	0.8	8.66
600	70	80.3	12.6	1.0	8.47

*Exposed to air

CONCLUSIONS

- Reactivity of low-rank coal chars are increased by factors of two to four at a given temperature with addition of catalyst.
- The increased reactivity is due to increases in surface area and active sites.
- Scanning electron microscopy shows that catalyzed chars have a much higher surface area than uncatalyzed chars.
- Potassium was distributed more uniformly than the trona over the char surface.
- The highly activated carbon created by the devolatilization of the low-rank coal necessitates the prevention of exposure to air if CO functional groups are to be accurately identified by ESCA or quantified by CP/MAS ^{13}C NMR.

REFERENCES

1. Pohani, B.P., J. Japan. Petrol. Inst., 27, 1 (1984).

2. Tomita, A., Y. Ohtsuka, Y. Tamai, Fuel, 62, 150 (1983).

3. Timpe, R.C., S.A. Farnum, S.J. Galegher, J.G. Hendrikson, M.M. Fegley, ACS Div. Fuel Preprints, 30, no. 4, p. 481 (1985).

4. Huttinger, K.J., R. Minges, Fuel, 65, 1112 (1986).

5. Sears, R.E., R.C. Timpe, S.J. Galegher, W.G. Willson, ACS Div. Fuel Preprints, 31, no. 3, 166 (1986).

6. Ratcliffe, C.T., Vaughn, S.N., ACS Div. Fuel Preprints, 30, no. 1, 304 (1985).

7. Botto, R.E., R. Wilson, and R.E. Winans, Energy and Fuels, 1, 173-181 (1987).

ACKNOWLEDGEMENTS

The authors would like to acknowledge Jan Lucht for assistance with the TGA experiments and Art Ruud for the ^{13}C NMR spectra. A special thanks is extended to Leland E. Paulson, Technical Project Officer, and Madhov Ghate, Chief, Combustion and Gasification Branch, of the Morgantown Energy Technology Center for their guidance and support.

a) Martin Lake Char - Mag. 6000X

b) Martin Lake/K_2CO_3

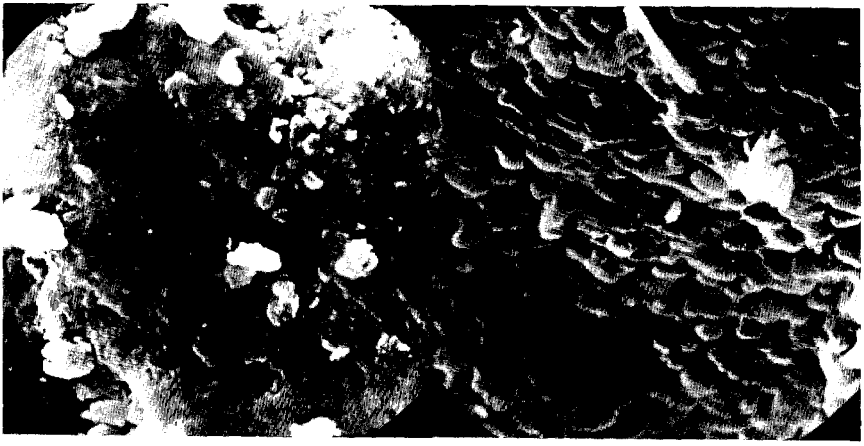

c) Velva Char - Mag. 6000X

d) Velva/M_2CO_3 Char - Mag. 6000X

Figure 1 - SEM Photographs of Coal Chars and Coal/K_2CO_3 Char Prepared at 750^{oC}

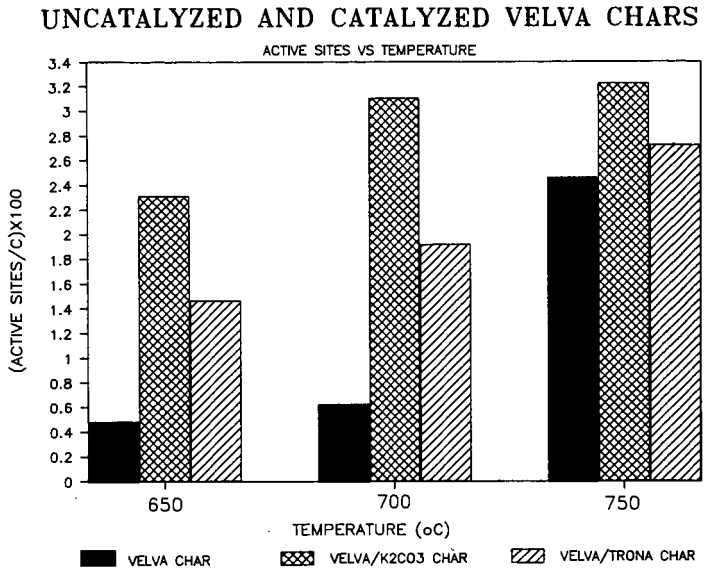

Figure 2. Number of active sites/carbon atom in Velva lignite char with and without catalyst.

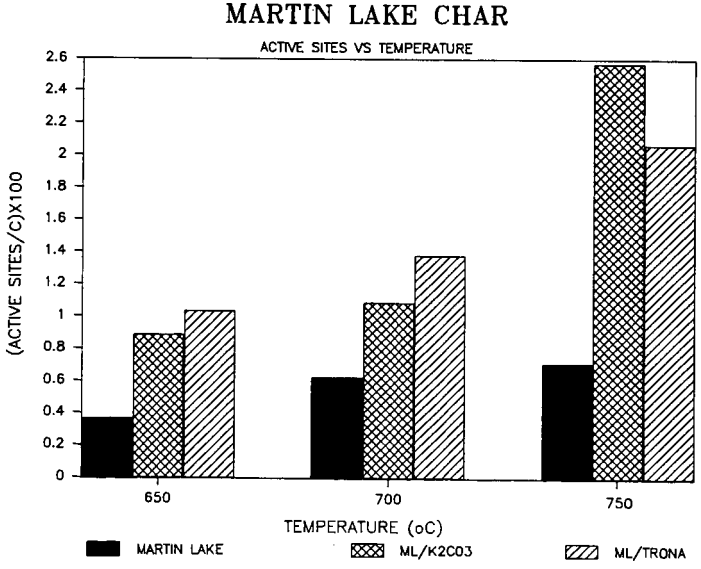

Figure 3. Number of active sites/carbon atom in Martin Lake lignite char with and without catalyst.

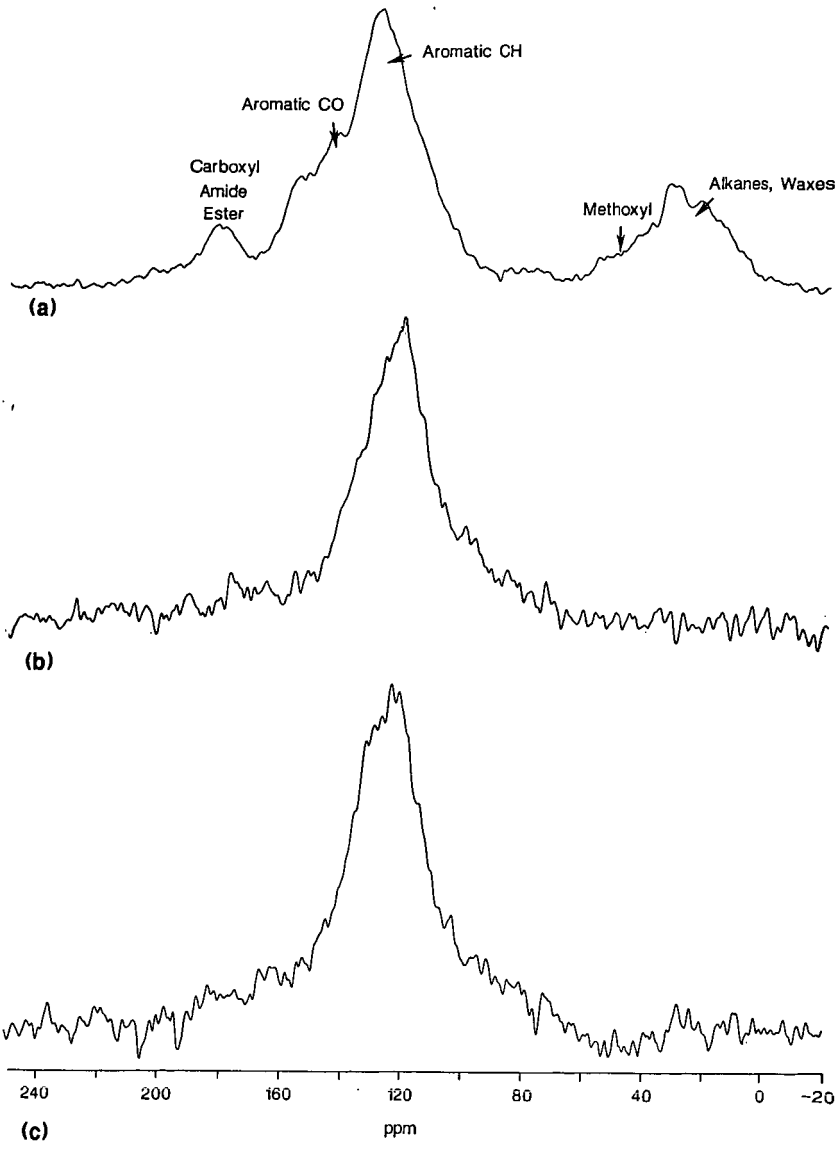

Figure 4. CP/MAS ^{13}C NMR Spectra of (a) Velva North Dakota lignite (b) Velva lignite char (750°C) and (c) Velva/Trona char 750°C.

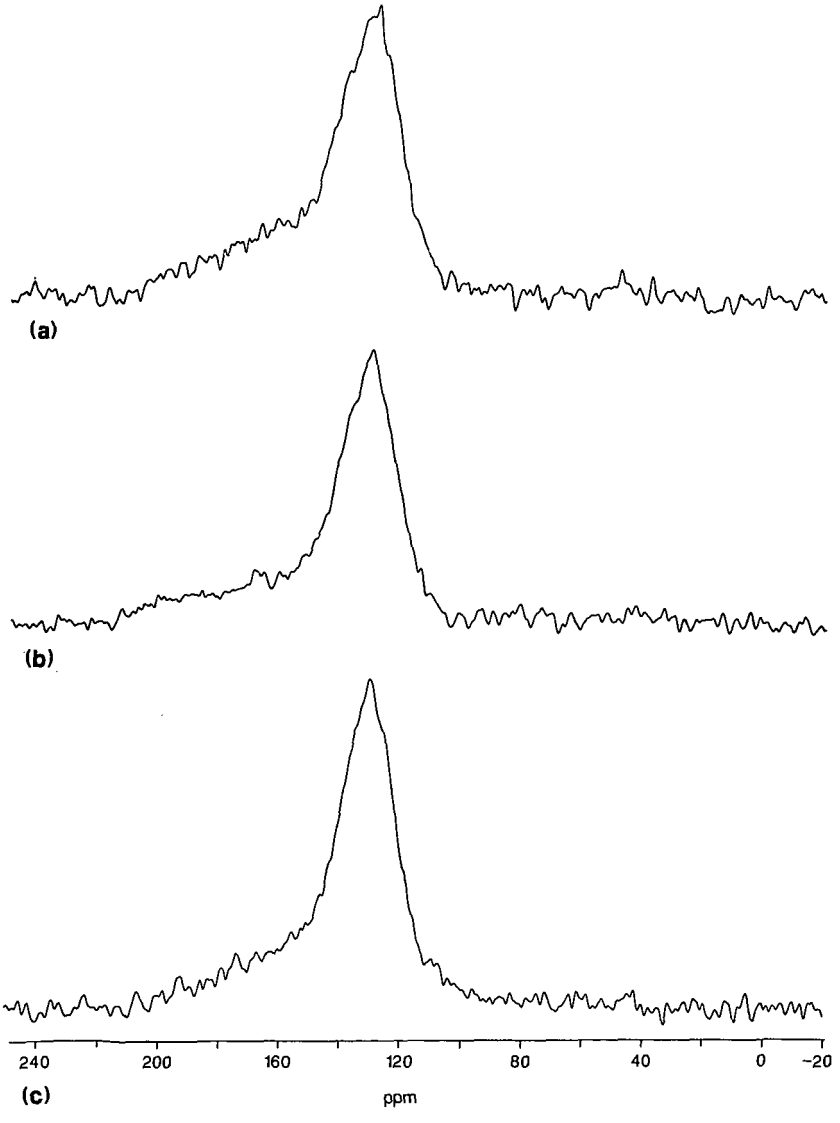

Figure 5. CP/MAS ^{13}C NMR spectra of Velva/Trona char prepared at (a) 700°C (b) 650°C, and (c) 600°C.

PYROLYSIS GC/MS ANALYSIS OF LOW-RANK COAL

David J. Miller and Steven B. Hawthorne

University of North Dakota Energy Research Center
Box 8213, University Station
Grand Forks, North Dakota 58202

ABSTRACT

The reactivity of coals under liquefaction conditions is related to their thermal decomposition. Pyrolysis GC/MS is used to determine the identity of the volatile products as the changes in coal structure occur. A Wyoming subbituminous coal (Clovis Point) and a North Dakota lignite (Indian Head) were heated under helium at four temperatures (160 °C, 250 °C, 300 °C, and 350 °C) for 30 minutes. The volatile species were cryogenically trapped in a capillary gas chromatographic column for GC/MS analysis. The two lower temperatures showed only devolatilization products (e.g., biological markers such as alkanes and terpenoids) while the higher temperatures yielded products resulting from bond-breaking (i.e., pyrolysis). The devolatilization and pyrolysis products of the two coals were similar in overall composition but markedly different in their distribution. The subbituminous coal (Clovis Point) pyrolysate contained phenol and cresols along with large amounts of C_{19} to C_{31} normal alkanes. Indian Head lignite pyrolysate contained a much larger amount of phenol, alkyl substituted phenols and dihydroxybenzene and lesser amounts of C_{19} to C_{31} alkanes.

INTRODUCTION

Pyrolysis gas chromatography/mass spectrometry has become increasingly popular for the analysis of solid fuel and fuel related materials. In recent papers, pyrolysis-GC/MS has been applied to model compounds (1), asphaltenes (2), kerogens (2), buried wood (3), coalified logs (3), and coal(4). A wide variety of techniques are employed for the pyrolysis of the sample. Most of the reported techniques employ some type of pyrolysis probe capable of rapid heating rates and temperatures in the 600 °C to >1000 °C range. The sample sizes reported were from 5 ug to 100 ug.

In order to study the products of thermal decomposition under low-severity liquefaction conditions, the maximum temperature used in this study was 350 °C. Our technique involves the use of approximately 10 mg of sample per analysis. The devolatilization and pyrolysis products are introduced into a split injector and cryogenically trapped at the head of a fused silica capillary gas chromatographic column. The use of a relatively large sample, 10 mg, and a split injector allows for a more representative sample to be collected on the capillary column. The sample is then separated and analyzed using standard GC/MS techniques.

EXPERIMENTAL

Samples

Wyoming subbituminous coal (Clovis Point) and a North Dakota lignite (Indian Head) were used in this study. Both coals were ground to -200 mesh and dried in a vacuum desiccator for 48 hours prior to pyrolysis.

Pyrolysis Gas Chromatography/Mass Spectrometry

Figure 1 shows a schematic diagram of the pyrolysis apparatus. Approximately 10 mg of coal was placed in a 30 cm x 4 mm i.d. pyrex tube. The sample was positioned approximately 5 cm from the outlet of the pyrex tube with a plug of silanized glass wool. The outlet of the tube was attached to a 1/4" x 1/16" stainless steel union fitted with a 2 in. x 0.20 mm i.d. needle. The sample tube was placed in the tube heater that had been preheated to the desired pyrolysis temperature. During the pyrolysis step, the needle was inserted into the split/splitless injection port, the helium flow was diverted from the injection port to sweep the pyrolysis products out of the pyrolysis chamber and into the injection port, and the tube heater was dropped down around the sample and union/needle assembly. The injection port was operated with a split ratio of approximately 1:100. The pyrolysate entering the fused-silica capillary chromatographic column was cryogenically trapped by holding the oven temperature at -50 ^{o}C during the 30 minutes pyrolysis. Upon completion of pyrolysis, the column oven was heated rapidly to 0 ^{o}C followed by temperature programming at 6 ^{o}C/min to 320 ^{o}C. GC/MS analysis of the pyrolysis products was performed with a Hewlett-Packard model 5985B using a 60 m x 0.25 mm i.d. (0.25 um film thickness) DB-5 fused silica capillary column (J & W Scientific, Folsom, CA). Helium was used as the carrier gas at an approximate linear flow rate of 50 cm/sec. Pyrolysis gas chromatography with flame ionization detection (GC/FID) was performed in a similar manner using a Hewlett-Packard 5890 GC.

Electron impact (EI) mass spectra were generated at 70 eV with a scan range of 35-500 amu. In the chemical ionization (CI) mode, reagent gas was introduced directly into the source through a heated transfer line colinear with the chromatographic column. Source pressure and CI tuning parameters have been reported previously (7). The structures of the dioxygen compounds (e.g., C_2 dihydroxybenzene vs C_1 methoxyphenol) were confirmed by the use of deuterated reagent chemical ionization GC/MS. In this technique, the -OH proton is exchanged for deuterium and an apparent molecular weight change occurs. For example, a C_2 dihydroxybenzene (MW = 138) would exhibit a pseudo-molecular ion at m/z 142 (ionization by D^+ and exchange of two acidic protons for deuterium), while a C_1 methoxyphenol (MW = 138) would have a pseudo-molecular ion at m/z 141 (ionization by D^+ and exchange of one acidic proton). Because of a prominent background ion at m/z

101 due to a reagent cluster ($(CH_3OD)_3D^+$), the lower limit for the mass scan range using CH_3OD CI was 104 amu.

RESULTS AND DISCUSSION

Figures 2 and 3 are the pyrolysis-GC/FID chromatograms of the Wyoming subbituminous coal and the North Dakota lignite at the four pyrolysis temperatures (160, 250, 300, and 350 °C). The numbered peaks in Figures 2 and 3 are identified in Table 1. Chromatograms for 160 °C and 250 °C show species that are thermally desorbed from the coal, and that are not pyrolysis products. This has been confirmed by the use of supercritical N_2O extraction (300 atm at 45 °C) (8) which yielded extracts that had chromatograms virtually identical to those from the 160 °C and 250 °C thermal experiments. These compounds are primarily biological markers such as alkanes, sesquiterpenes, triterpanes and steranes(5,6).

Comparison of the chromatograms obtained at 350 °C for the two coals shows marked differences in the composition of their pyrolysates. The pyrolysate yield for the lignite under the pyrolysis conditions described in the experimental section was much less then the yield for the subbituminous coal. The pyrolysate from the Wyoming subbituminous coal contains relatively larger amounts of aliphatics, aromatics, and oxygen-containing species such as phenol and alkylphenols. Catechol (1,2-dihydroxybenzene) is present in the pyrolysate of both coals, but in much lower concentration from the subbituminous coal than from the lignite. The lignite pyrolysate contains the same types of compounds as those found in the subbituminous coal pyrolysate but the distribution is very different. Alkanes in the range of C_{18} to C_{31} are present in both pyrolysates but are in much lower concentration in the lignite pyrolysis product. Anisole and C_1 anisole isomers were present in the lignite pyrolysate but not in the subbituminous pyrolysate. Larger amounts (relative to other components in the sample) of dihydroxybenzene, methoxyphenol, and their C_1 and C_2 alkyl derivatives were present in the lignite pyrolysate. This is consistent with results published by Hatcher, et al (3), and would be expected since lower rank coals have undergone less coalification and would contain organic constituents which more closely resemble structures (e.g., lignin) found in the original plant material. Several of the substituted dihydroxybenzenes and methoxyphenols were absent from the subbituminous pyrolysate.

CONCLUSION

Pyrolysis gas chromatography/mass spectrometry can be a valuable tool for evaluating candidate coals for use in synthetic fuel processes especially where separation and upgrading of the pyrolysate fraction is a concern and the chemistry of the process has a narrow operational range. Structural differences in the pyrolysates can be related to the structure of the coals. The larger sample size and split injection used in our technique

allows for a more representative sample to be analyzed.

CREDIT

The authors would like to thank the U.S. Department of Energy for support for this work under contract number DE-FG22-86PC90911.

REFERENCES

1. Bredael, P. and Vinh, T. H., Fuel, 58, 211-214 (1979).

2. Solli, H., and Leplat, P., Org. Geochem., 10, 313-329 (1986).

3. Hatcher, P. G., Lerch, H. E., Kotra, R. K., Verheyen, T. V., ACS Div. Fuel Chem. Preprints, 32(1), 85-93 (1987).

4. Siskin, M. and Aczel, T., Fuel, 62, 1321-1326 (1983).

5. van Graas, G., Org. Geochem., 10, 1127-1135 (1986).

6. Strachan, M. G., Alexander, R., Kagi, R. I., ACS Div. Fuel Chem. Preprints, 31(3), 266-274 (1986).

7. Hawthorne, S. B., and Miller, D. J., Anal. Chem., 57, 694-698 (1985).

8. Hawthorne, S. B., and Miller, D. J., Anal. Chem., (accepted for publication in June 1987).

TABLE I. Identification of Numbered Peaks from Figures 2 and 3.

Peak Number	Species
1	methylcyclopentadiene or isomer
2	benzene
3	acetic acid
4	C_2-cyclopentadiene or isomer
5	toluene
6	C_2-cyclohexane or isomer
7	C_2-benzene
8	cyclooctatetraene and C_2-benzene
9	anisole
10	phenol
11	C_1-anisole
12	C_3-benzene
13,14	cresol isomers
15	methoxyphenol
16	C_2-phenol
17	dihydroxybenzene
18	C_3-benzene
19	C_1-dihydroxybenzene and C_1-methoxyphenol
20	C_1-dihydroxybenzene
21,22	C_2-dihydroxybenzene
23	C_2-naphthalene
24	cadalene
25	M=266 biological marker
26-39	C_{18} to C_{31} alkanes
40,41,42	M=206 sesquiterpene isomers
43	M=262 biological marker
44	M=276 biological marker
45	M=270 biological marker
46	M=252 biological marker
47	M=234 biological marker
48	M=286 biological marker

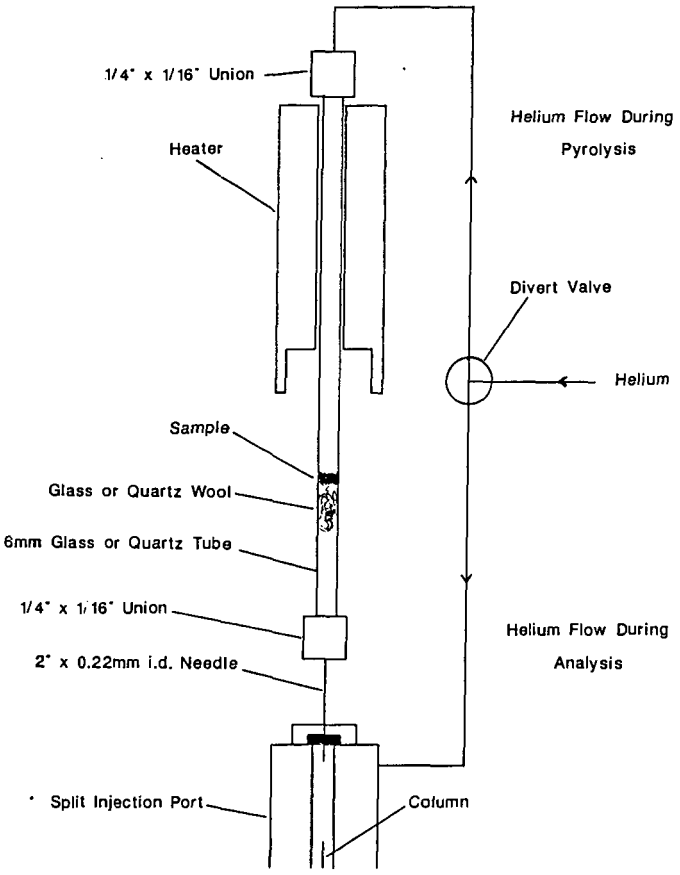

Figure 1. Pyrolysis Apparatus.

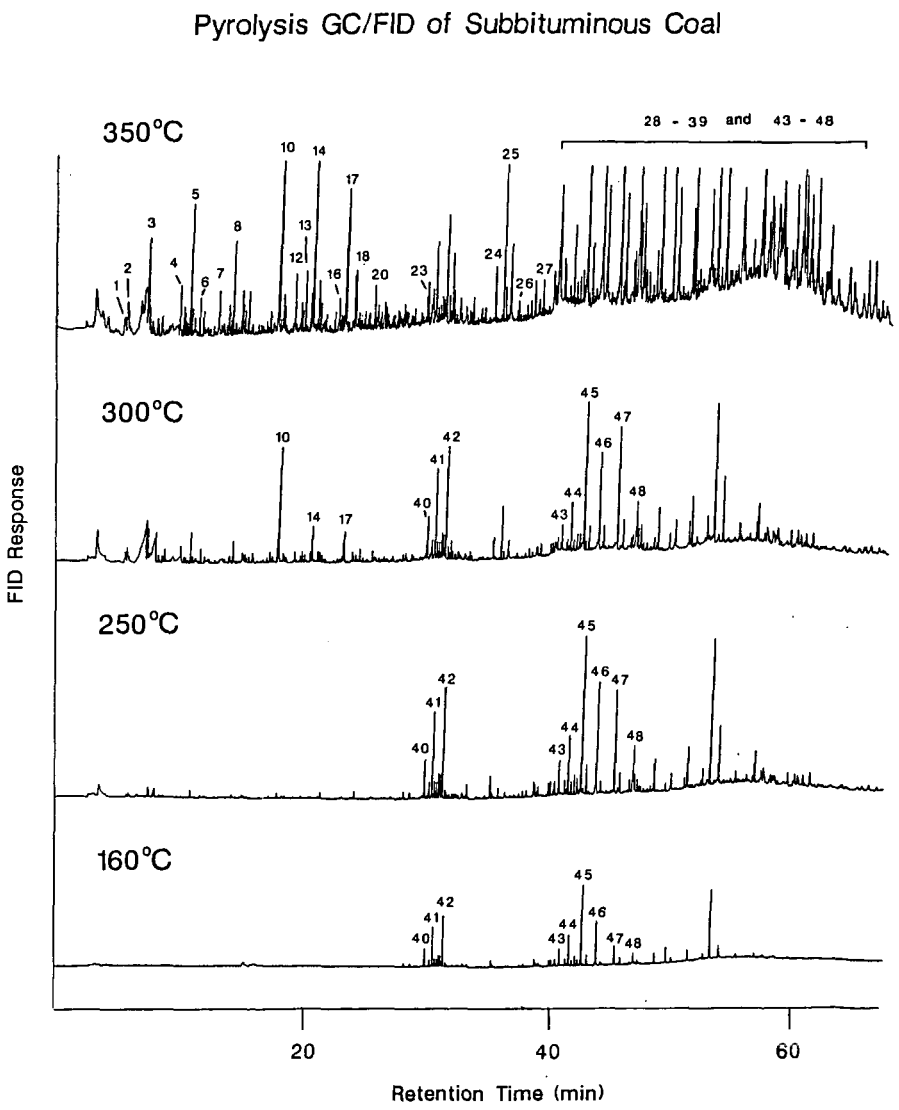

Figure 2. Pyrolysis GC/FID trace from Wyoming subbituminous coal.

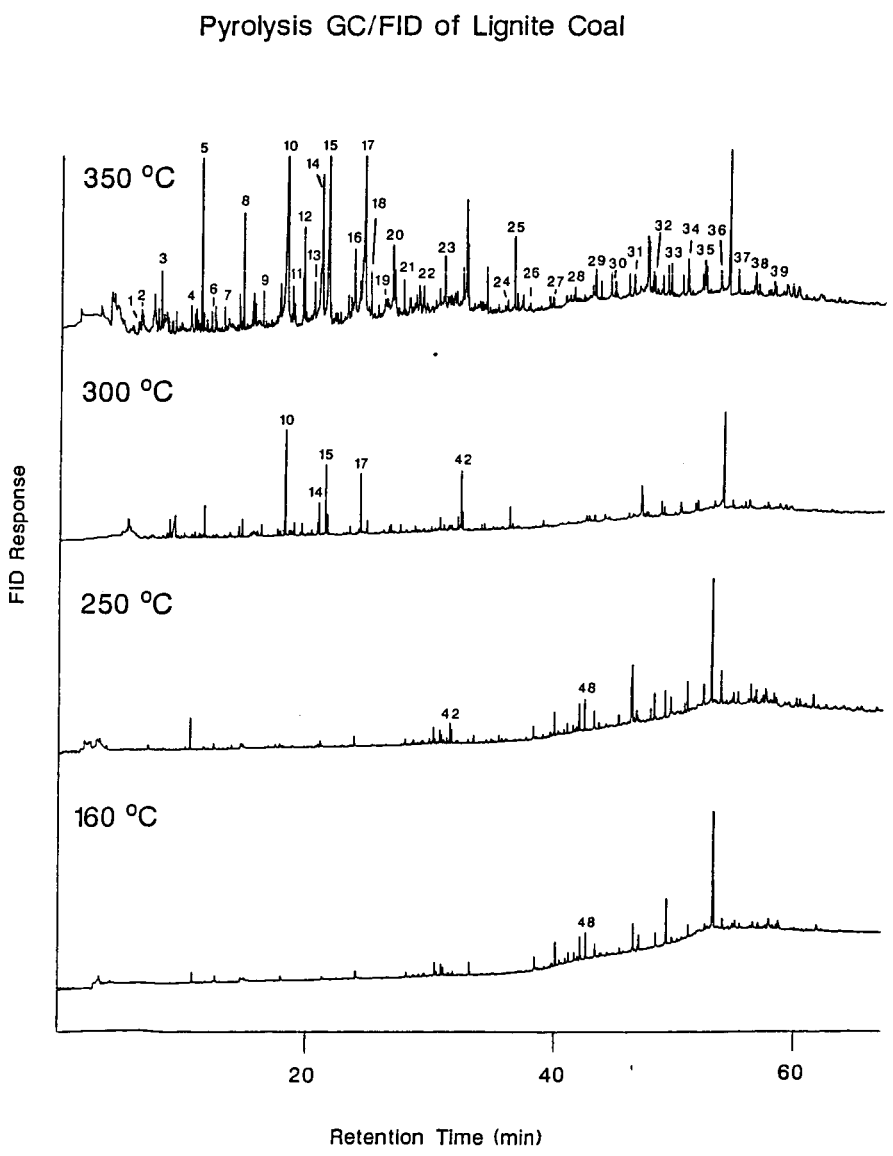

Figure 3. Pyrolysis GC/FID trace from North Dakota lignite.

COMPARISON OF DETECTORS FOR SIZE EXCLUSION CHROMATOGRAPHY OF HEAVY OIL FRACTIONS

S. COULOMBE

CANMET, Energy Research Laboratories
Energy, Mines and Resources Canada
555 Booth Street, Ottawa, Ontario K1A 0G1

INTRODUCTION

Size exclusion chromatography (SEC) is often used for the molecular weight determination of heavy oils, residues, pitches and asphaltenes because it is capable of providing the molecular weight distribution in addition to the average molecular weights. However, since these samples are very complex, results are often approximative because of three factors. First, the exclusion process separates molecules by size and shape instead of weight. Second, the sample is composed of hundreds of molecules having widely different properties which implies that additional interactions will add to the size exclusion process (1-4). Finally, the quantitation itself is approximative since usual LC detectors do not provide a signal that is independant of the molecular structure.

In this paper, the performance of a differential refractometer, an evaporative detector and a flame ionization detector for liquid chromatography is compared in terms of linearity, response factors and detection limits.

EXPERIMENTAL

The refractive index detector is a Waters 401 differential refractometer used in conjunction with a thermostated bath to keep the detector in isothermal conditions.

The flame ionization detector is a Tracor 945 LC-FID specially designed for liquid chromatography. The eluant is deposited on the belt and the solvent is evaporated before the belt enters the detector flame which will detect only the solute.

The evaporative detector is an Applied Chromatography System (ACS) 750/14 "Mass Detector" in which the eluant is nebulized at the entrance of a heated tunnel. The solvent is evaporated in this tunnel, thus leaving solute particles in a gas stream. Light scattered by the non-gaseous particles is detected by a photomultiplier.

Experiments were performed on a Varian 5000 liquid chromatograph using two types of columns: a Techsphere 5um amino column (HPLC Technology Ltd) for light standards and three Ultrastyragel styrene/divinylbenzene GPC columns (Waters) for polymer standards. All solvents were degassed before use.

RESULTS

Results are presented in terms of response factors, detection limits and linearity. Response factors are calculated according to the following equation:

$$RF = \frac{\text{area under peak X}}{\text{amount of compound X}} * \frac{\text{amount of standard}}{\text{area umder standard peak}}$$

Detection limit (DL) is calculated as the amount of compound equivalent to twice the noise level. In order to take account of different retention times and peak shapes, a time corrected detection limit (DLT) was defined as the detection limit (DL) divided by the peak width at half-height.

Finally, the linearity range was evaluated using log-log graphs of peak area vs injected amount for concentrations ranging from detection limit to solubility limit at room temperature.

Differential refractometer

This detector is the most widely used in size exclusion chromatography. Table 1 shows how response factors can vary from compound to compound. This can obviously cause errors in quantitation. Detection limits were calculated for two extreme compounds avoiding cases where solubility problems were suspected. Finally, Figure 1 shows excellent linearity over three orders of magnitude for phenanthrene.

Flame ionization detector

Figure 2 shows the signal decrease observed with time for a series of injections of a four-component mixture. Note that the time scale is not linear nor proportional. The numbers only indicate the order of injection. Pearson and Gharfeh (10) found that this decrease was caused by a gradual overheating of the block supporting the belt, thus causing evaporation of the solute before it gets to the flame. They proposed to use a fan to keep a good ventilation. In our experiments, an internal standard was used to calculate the response factors and calculations of detection limits were done on early injections.

Table 2 shows how response factors can vary between compounds. Linearity (Fig. 3) is good if one avoids high concentrations where low response was probably due to detector saturation. However, it must be noted that the relation is exponentional as shown by the slope different than 1.

Evaporative detector

Temperature is the most important operating parameter of this detector. Ideally, the evaporation tunnel is maintained at a temperature which will ensure complete evaporation of the solvent while the solute is not affected by the process. This temperature

setting is not in degrees but in arbitrary units, 0 meaning no heating. Figure 4 shows that a high temperature setting can seriously affect the response and how the variation is closely related to the molecular weight (or boiling point) of the compound. One must note here that standards selected for this study are not particularly volatile since their molecular weight is higher than 165 g/mol and their boiling point >285°C. Bartle (6) also stated that the analysis of samples having a molecular weight lower than 300 g/mol is questionable.

Response factors were calculated for several temperature settings (Table 3). At higher temperatures, response factors are extremely different. When no heating is applied, differences are less severe but still very significant. It can be observed that even without heating the response factors are still correlated with boiling points although these are relatively high (>285°C). Of course, detection limits vary to the same extent (Table 4).

Linearity plot (Fig. 5) shows some curvature. However, if one avoids a lower concentration range, the curve could be approximated to an acceptable straight line whose slope is closer to 1, which facilitates calibration. Oppenheimer and Mourey (8) already indicated that operating conditions must be carefully chosen in order to ensure linear relationship. Along with Charlesworth (5,7), they also indicated that aerosol formation influences detection. Hence, surface tension and viscosity of the solvent are important since the droplet size will influence the size of the particles that cross the light beam. It is also possible that the refractive index (7,8) and opacity of these particles have a significant influence on the output signal.

Polymers

Since the evaporative detector is mainly used in polymer analysis, response factors and linearity were investigated for selected polymers. Response factors for these polymers seem to be more uniform than for the refractometer, and also more uniform than for the individual standards analyzed in previous sections (Table 5). Linearity (Fig. 6) appears to improve slightly with polymers but again it is preferable to avoid concentrations approaching detection limits.

DISCUSSION

Performance

Linearity (Fig. 1, 3, 5 and 6) is definitely better for the refractometer than for the other detectors. Both LC-FID and evaporative detector linearity plots show curvature that could be avoided if not working with too high or too low concentrations. In the case of LC-FID, the response is clearly exponential and one must be careful in using a calibration curve.

Table 6 shows a summary of the variation of response factors for a series of components. For individual standards of molecular weight

between 165 and 300 g/mol, the refractometer showed the least scatter of data as the relative standard deviation (RSD) indicates. The evaporative detector gave the worst results because the evaporation of solute was a limiting factor. When polymers are considered, this detector seems to be slightly superior to the refractometer since evaporation of sloute is minimal.

The variety of response factors obviously influences detection limits (Table 7). However, minimum and maximum values give an overview of the range that can be expected for a given detector. One can see that the LC-FID has detection limits one order of magnitude higher than the other detectors due to high noise levels and spiking problems (see Fig. 7).

Other characteristics

The refractometer cannot be operated in a solvent gradient mode. This is not really a problem in SEC since gradients are seldom used with this type of chromatography. The nature of the detection process also implies that response factors thus quantification might be different when using different solvents. On the other hand, the refractometer is a very simple and easy-to-use detector showing good reproducibility. A definite advantage over the two other detectors is that it is suitable for both light and heavy compounds.

The evaporative detector response is partly related to the quality of the aerosol thus to physical properties of the eluant. These properties are affected by operating temperature, pressure, flow rate and solvent. For this reason, one must be careful in using gradients. As mentioned previously, volatile compounds cannot be analyzed using this detector. Finally, the evaporative detector is solid and relatively easy to use.

In comparison, the LC-FID is a fragile detector, especially the belt. It is more complicated to operate. However, once good conditions are found, they do not have to be changed. One could question the completeness of detection and of combustion by the cleaning flame when heavy compounds are analyzed.

Analysis of pitch samples

Table 8 shows the results obtained for the SEC analysis of three pitch samples while comparative chromatograms for sample 1 are given in Fig. 7. A ultraviolet detector trace was added for comparison. Obviously, a UV detector is not recommended since the extinction coefficient can be widely different between components. It can be seen here that it overestimates the contribution of the high molecular weight portion of the sample. This is indicated by very high weight average molecular weight (M_w) values since more importance is given to heavier species in the calculation of M_w. Conversely, the LC-FID does not detect high molecular weight species very well as shown by the lower M_w values. This detector also displayed severe spiking and high systematic noise that were responsible for the poor detection limits.

As shown in Table 8, average molecular weght values can differ widely and moreover the trends between samples are not always the same (see M_n for samples 2 and 3). Figure 7 shows that the refractometer detects a larger quantity of heavy material than other detectors (except UV) and that detection of the light material with the refractometer can be disturbed by the solvent front. On the other hand, the lighter components might not be detected properly by the evaporative detector. Finally, the noise level is slightly lower for the refractometer than for the evaporative detector.

SUMMARY

When considering all factors, it is very difficult to select a specific detector as the best for size exclusion chromatography of heavy oil related samples. The LC-FID was found to be unsatisfactory. The only procedure that would aid the selection between the refractometer or the evaporative detector would be to collect and weigh narrow fractions of the chromatographic effluents and to calculate the molecular weight of these less complex fractions. However, this time consuming procedure would have to be repeated for different types of samples. Current practice in our laboratory is to analyze samples with both detectors in series in order to get a better idea of the nature of the sample.

REFERENCES

1. Altgelt, K.H. in Chromatography in Petroleum Analysis, Chromatogr. Sci. Ser., v.11, 1979, p.287.

2. Cazes, J., Gaskill, D.R., Proceedings of the 6th International Seminar on Gel Permeation Chromatography, Miami Beach, Oct. 1968, p.147.

3. Albaugh, E.W., Talarico, P.C., J. Chrom., 74, 233, 1972.

4. Champagne, P.J., Manolakis, E., Ternan, M., Fuel, 64, 423, 1985.

5. Charlesworth, J.M., Anal. Chem., 50, 1414, 1978.

6. Bartle, K.D., Taylor, N., Mulligan, M.J., Mills, D.G., Gibson, C., Fuel, 62, 1181, 1983.

7. Mourey, T.H., Oppenheimer, L.E., Anal. Chem., 56, 2427, 1984.

8. Oppenheimer, L.E., Mourey, T.H., J. Chrom, 323, 297, 1985.

9. Dixon, J.B., Chimia, 38, 82, 1984.

10. Pearson, C.D., Gharfeh, S.G., Anal. Chem, 58, 307, 1986.

Table 1 - Response factors and detection limits for differential refractometer

Compound	RF	DL (10^{-7} g)	DLT (10^{-8} g/s)
Pyrene	1.0		
Phenanthrene	0.94	2.8	3.3
o-Terphenyl	0.74		
3-Methyl cholanthrene	0.95		
Dibenzofuran	0.74		
Benzophenone	0.65		
Xanthene	0.75		
Eicosanol	0.25		
Diphenyl amine	0.78		
5,6-Benzoquinoline	0.85		
Carbazole	0.34		
Dibenzothiophene	0.84		
Thianthrene	0.72		
Triphenyl methyl mercaptan	0.52	11.3	18.9

Table 2 - Response factors and detection limits for flame ionization detector

Compound	RF	DL (10^{-6} g)	DLT (10^{-7} g/s)
Pyrene	1.0		
Phenathrene	0.21		
o-Terphenyl	0.86		
3-Methyl cholanthrene	0.78		
n-C_{21}	1.58		
Dibenzofuran	0.26	4.2	3.5
Benzophenone	0.54		
Xanthene	0.54		
Eicosanol	0.87		
Diphenyl amine	0.30		
5,6-Benzoquinoline	0.59		
Carbazole	0.12		
Dibenzothiophene	0.69		
Thianthrene	0.99	2.6	2.2
Triphenyl methyl mercaptan	0.26		

Table 3 - Response factors for evaporative detector

Compound	Temperature setting			
	0	5	10	15
Pyrene	1.0	1.0	1.0	1.0
Phenanthrene			0.26	0.21
o-Terphenyl	0.53	0.46	0.31	0.62
3-Methyl cholanthrene	0.85	1.57	1.43	5.21
$n\text{-}C_{21}$			0.69	1.69
Dibenzofuran	0.027	0.014	0.011	0.004
Benzophenone	0.13	0.073	0.083	0.040
Xanthene			0.060	0.047
Eicosanol			0.80	2.75
Diphenyl amine			0.11	0.064
5,6-Benzoquinoline			0.60	0.34
Carbazole			0.76	2.45
Dibenzothiophene	0.19	0.12	0.15	0.12
Thianthrene			0.25	0.32
Triphenyl methyl mercaptan			1.04	1.94

Table 4 - Detection limits for evaporative detector

Compound	DL (10^{-6} g)				DLT (10^{-7} g/s)			
Temperature:	0	5	10	15	0	5	10	15
Dibenzofuran	2.11	37.3			3.51	62.2		
Benzophenone	1.55	14.6	9.84	34.8	1.04	9.76	8.2	29.1
Pyrene	0.741	2.24	1.73	3.45	0.617	1.87	1.44	2.88
3-Methyl cholanthrene	0.575	1.01	1.06	1.06	0.319	0.564	0.588	0.588

Table 5 - Response factors for polymers

Compound	Refractometer	Evaporative detector
Polystyrene	1.0	1.0
Polyvinyl acetate	0.19	0.44
Polysulfone	0.92	0.71
Polyethylene glycol	0.31	0.67
Polyamide	0.34	0.35
$n\text{-}C_{36}$	0.18	0.61

Table 6 - Summary of response factors

Detector	Min	Max	n	X		RSD
Standard compounds						
Refractometer	0.25	1.0	14	0.72	0.22	31%
Flame ionization	0.12	1.58	15	0.64	0.39	61%
Evaporative (T=0)	0.027	1.57	6	0.45	0.40	89%
detector (T=10)	0.011	1.43	15	0.50	0.43	86%
Polymers						
Refractometer	0.18	1.0	6	0.49	0.37	76%
Evaporative det. (T=0)	0.35	1.0	6	0.63	0.23	36%

Table 7 - Summary of detection limits

Detector	DL (ug/g)		DLT (ng/s)	
	Min	Max	Min	Max
Refractometer	0.28	1.13	33	189
Flame ionization	2.6	4.2	220	350
Evaporative det. (T=0)	0.58	2.1	32	35
(T=5)	1.0	37	56	6200

Table 8 - Average molecular weight of pitch samples

Sample	Refractometer	Evaporative det.	LC-FID	UV
	Number average molecular weight, M_n			
1	780	590	560	580
2	500	380	470	290
3	290	340	330	250
	Weight average molecular weight, M_w			
1	2730	1960	1050	3410
2	2250	1520	880	2540
3	2170	1380	630	2240

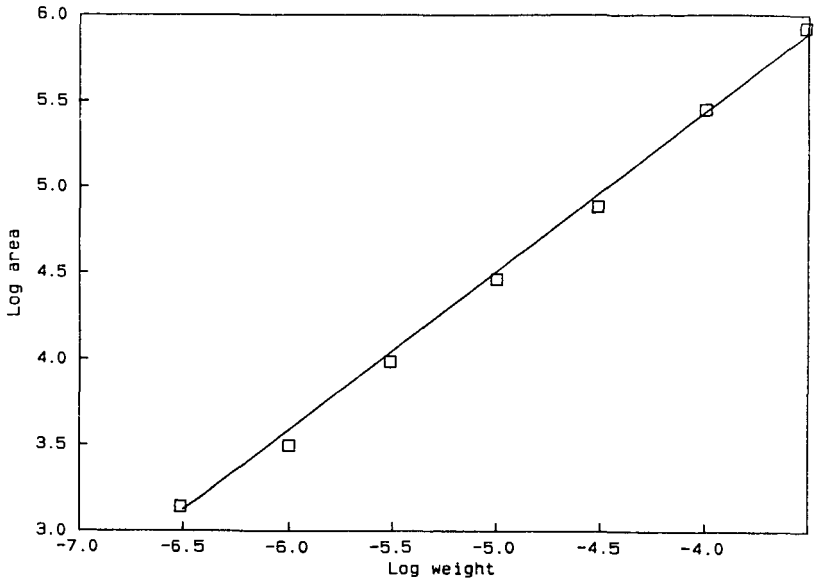

Fig.1 - Linearity of refractometer for phenanthrene (Slope=0.941, r=0.9988)

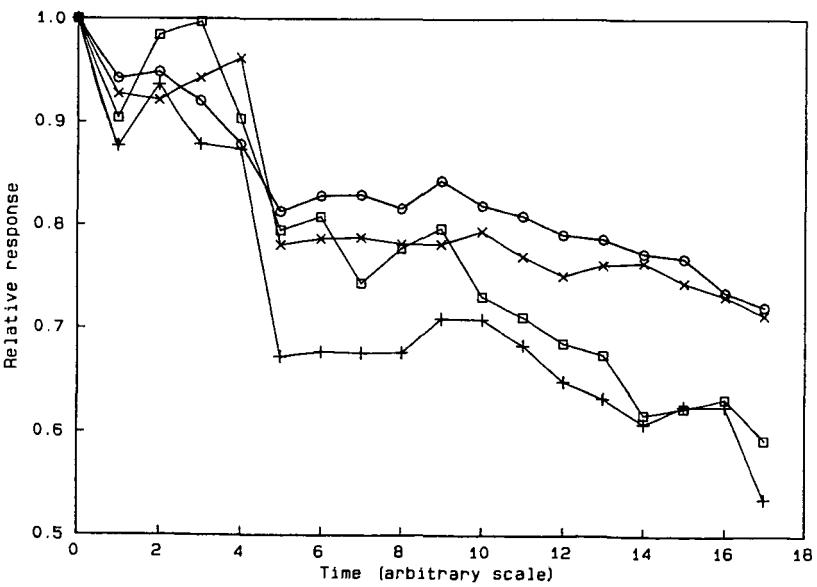

Fig.2 - Variation of signal with time for LC-FID (□ dibenzofuran, + dibenzothiphene, ○ pyrene, X benzophenone)

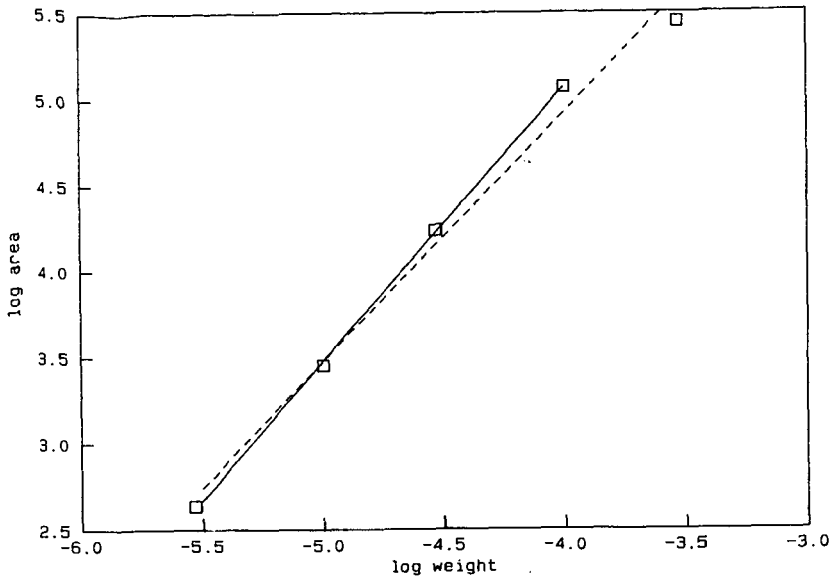

Fig.3 - Linearity of LC-FID for thianthrene (--- : slope=1.447, r=0.9946; ——— : slope=1.594, r=0.9999)

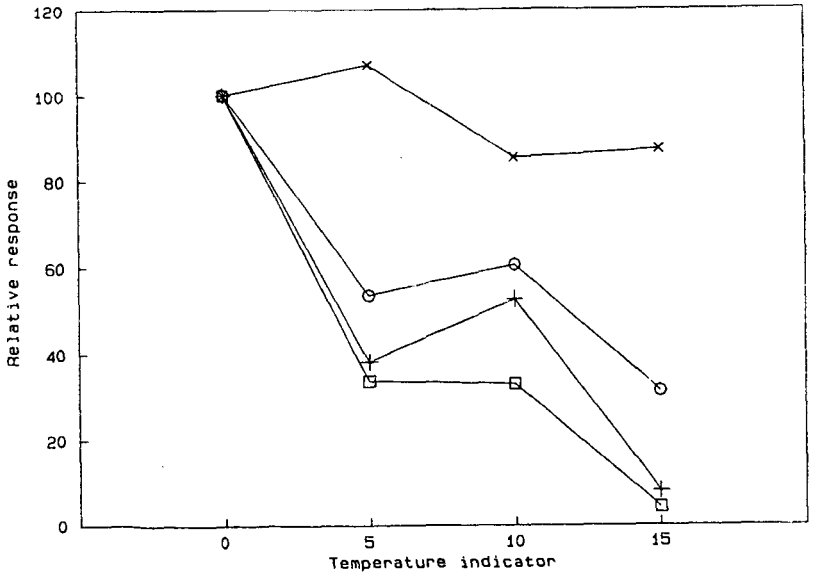

Fig.4 - Relative variation of signal with temperature setting of evaporative detector: □ dibenzofuran (MW=168), + benzophenone (MW=182), O o-terphenyl (MW=230), X 3-methyl cholanthrene (MW=268)

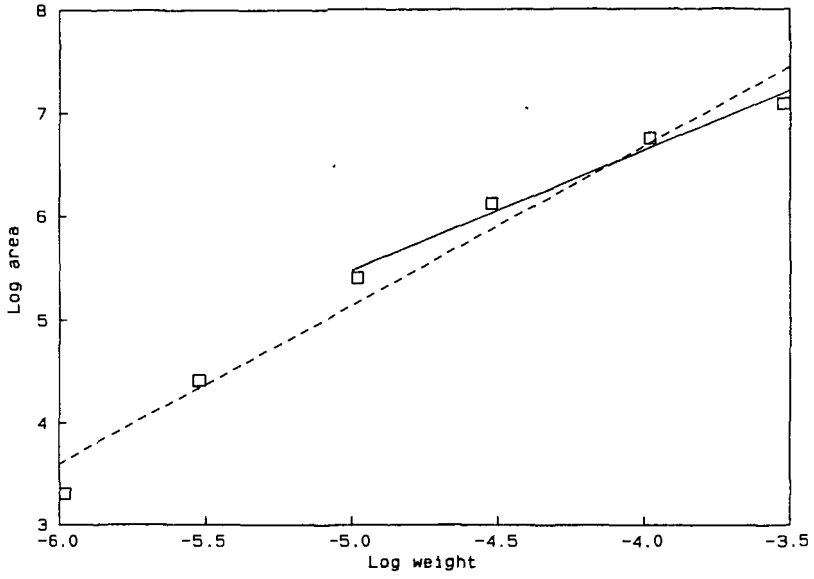

Fig.5 - Linearity of evaporative detector for pyrene (--- slope=1.537, r=0.9839;—— slope=1.161,r=0.9892)

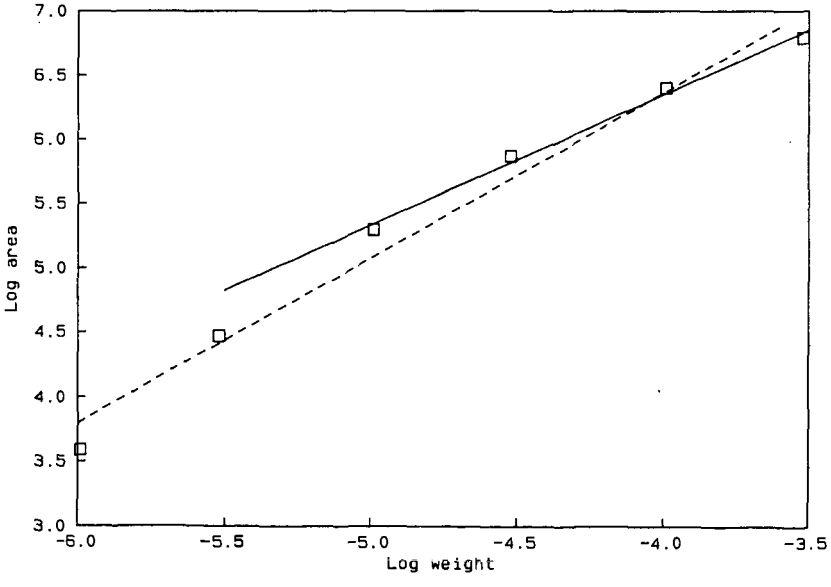

Fig.6 - Linearity of evaporative detector for polystyrene of M_w=6200 (--- slope=1.286, r=0.9888;—— slope=1.011, r=0.9969)

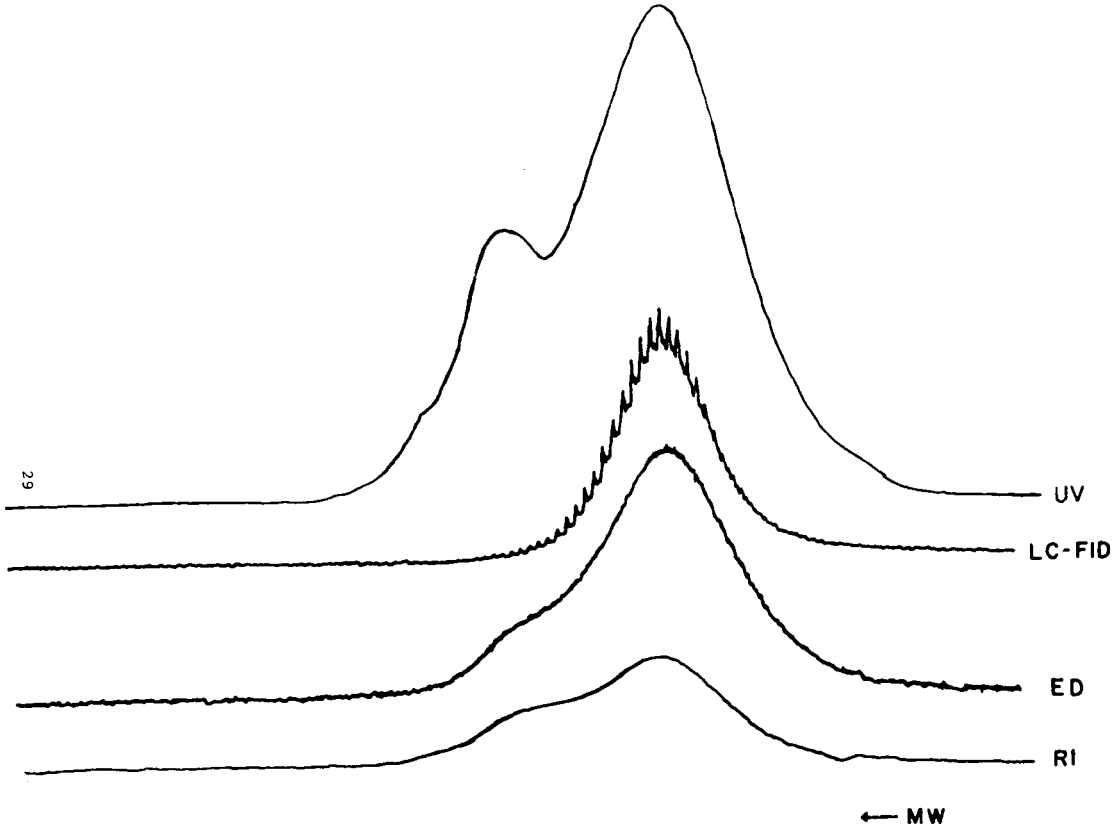

Fig.7 - SEC chromatogram of a pitch sample as detected by different detectors (UV = ultraviolet, LC-FID = flame ionization detector for liquid chromatography, ED = evaporative detector, RI = refractometer)

DETERMINATION OF AROMATICS IN HEATING OILS AND DIESEL FUELS BY SUPERCRITICAL FLUID CHROMATOGRAPHY

B.J. Fuhr, L.R. Holloway & C. Reichert

Alberta Research Council, Box 8330, Stn F
Edmonton, Alberta, Canada T6H 5X2

S.W. Lee & A.C.S. Hayden

Energy, Mines & Resources Canada, CANMET, 555 Booth Street
Ottawa, Ontario, Canada, K1A 0G1

INTRODUCTION

The presence of high quantities of aromatic compounds in middle distillate fuels causes problems for refiners and users because of the sooting propensity of such oils. Distillate fuels containing a high proportion of aromatic compounds are being produced due to the increased use of non-conventional crudes and of lower cost blending components to maximize product yield.

The method normally used in refineries for determining aromatics in oils is ASTM D 1319, the fluorescent indicator adsorption (FIA) method (1). The method uses inexpensive equipment and is simple to perform; however, it does have some limitations. The procedure is lengthly and results depend upon the operator's ability to distinguish between the colored bands, which can be difficult for colored samples. Problems have been reported with variations in dye composition and availability of the proper grade and activity of silica gel (2). Finally, the scope of the method excludes samples with final boiling points greater than 315°C.

The purpose of the present work was to develop a simple, inexpensive and precise method to determine aromatics content in heating oils and diesel fuels. It was desired that the method be applicable to samples boiling as high as 400°C, and that it be suitable for use in refinery control laboratories.

Mass spectrometry and nuclear magnetic resonance may be used for aromatics determination, but both require expensive instrumentation and highly trained operators. They are therefore unsuitable for routine refinery use.

Many methods based on high performance liquid chromatography (HPLC) have been employed for saturates and aromatics determination. Some examples are those reported by Suatoni and Swab (3), Alfredson (4) and Cookson et al (5). Generally these methods are characterized by good separation, analysis times of less than 10 minutes, and are not limited to low boiling samples. Their main disadvantage is the specificity of the usual ultraviolet (UV) and refractive index (RI) detectors, which require extensive calibration using either model compounds similar to those in the samples being analyzed, or fractions prepared from the actual samples by open column chromatography.

Two detectors thought to be preferable to the RI and UV, because of their relative uniformity of response for hydrocarbon types over a wide range of carbon numbers, are the dielectric constant (DC) detector and the flame ionization detector (FID). This uniformity of response greatly simplifies the calibration procedure. Hayes and Anderson (6) used a DC detector in conjunction with conventional HPLC

employing Partisil columns and n-butylchloride as the mobile phase to determine saturates, monoaromatics and polyaromatics in fuel distillates.

The FID presents a problem when used with conventional HPLC because of interference from commonly used solvents. Norris and Rawdon (2) have successfully coupled supercritical fluid chromatography (SFC) with FID using carbon dioxide as the mobile phase and a silica column coated with silver nitrate to determine saturates, olefins and aromatics in gasolines. Schwartz and Brownlee (7) also employed SFC/FID to determine paraffins, olefins and aromatics in gasolines employing a silica column with sulfur hexafluoride as the mobile phase.

In SFC the mobile phase is a highly compressed gas (8) with excellent solvating properties. This condition is achieved above the critical temperature and pressure of the mobile phase. Generally the density of the fluid and hence its solvating ability is increased by either increasing the pressure or decreasing the temperature. This will usually result in a loss of selectivity within a homologous series, but can be advantageous when class separations (saturates, aromatics) are desired over a wide molecular weight range. An SFC system is easily coupled to an FID with little interference from the mobile phase fluid since it rapidly desolvates before entering the detector (9).

In the present work the effects of temperature, pressure and stationary phase on the SFC/FID determination of aromatics in middle distillate fuels were investigated. The FID response to both saturates and aromatics isolated from several actual samples was determined. Results were compared to those obtained by the FIA method, and the possibilities of using SFC/FID for determining aromatics on the basis of number of rings was investigated.

EXPERIMENTAL

Instrumentation

A Varian model 8500 syringe pump was used to pressurize the carbon dioxide in the chromatographic column. Inlet pressures were between 3250 and 4200 psi (22,400 and 28,900 kPa). To facilitate filling of the pump with liquefied gas, two alternate methods were used. One employed a Lauda model K4R circulator bath to keep the syringe pump cooled. The other employed a cylinder of carbon dioxide pre-pressurized to 1200 psi with helium which allowed the pump to be filled without cooling (10). A Shimadzu model GC-8A gas chromatograph equipped with an FID contained the chromatographic column. The GC was run isothermally at temperatures ranging from 35 to 90°C; the temperature of the detector was 400°C. A Rheodyne valve model 7520 equipped with a 0.2 μL internal sample loop mounted on the exterior of the gas chromatograph was employed to introduce the sample onto the column. A Spectra-Physics model 4290 computing integrator was used for the collection and reduction of the data.

Columns and Restrictors

All columns were 250mm x 2.1mm ID (Alltech Associates). The following stationary phases were employed: 5μ silica adsorbosphere, 5μ cyano, 5μ amino, and 20% $AgNO_3$ on 5μ silica. The restrictors were flexible fused silica capillary tubing attached to the column with a 0.4mm 40% graphite ferrule with a low dead volume fitting. Either 50mm of 10μ ID tubing inserted approximately 30mm into the FID, or 130mm of 20μ ID tubing inserted approximately 90mm into the FID, as close as possible to the flame, was used. The latter arrangement was found to eliminate "spiking", a common problem in SFC (10).

Chemicals and Calibration Materials

Fisher Scientific ACS grade carbon disulfide (CS_2) was used for dilution of the samples. A modification of the column chromatographic procedure of Sawatzky et al (11) was used for the preparation of saturates and aromatics fractions from several actual samples. The saturates fraction was eluted from the silica-alumina column with n-pentane and the aromatics with toluene. Following careful air drying to remove the solvent these fractions were used for checking the FID response factors.

RESULTS AND DISCUSSION

Saturates-Aromatics Separation

A. Effect of Temperature: Retention time data, expressed as capacity factors, for a series of model compounds are shown in the first two columns of Table 1 for the silica stationary phase, mobile phase pressure of 3600 psi and temperatures of 90 and 35°C. The capacity factor, k, is defined by:

$$k = (t_R - t_o) / t_o$$

where t_R is the retention time of the given model compound, and t_o is the retention time of a compound not retained by the column which in this case is the impurity peak in the CS_2 solvent. At both temperatures, the saturates span a much smaller range of k values than do the aromatics. However, it can be seen that at 35°C the saturates as a group are better separated from the monoaromatics. For example at this temperature C_{30} has a lower k value than does benzene, but at 90°C C_{20} and toluene have approximately the same k values. The boiling points of toluene and C_{30} correspond approximately with the lowest initial boiling point and the highest final boiling point (as determined by gas chromatographic simulated distillation) of all middle distillate samples studied in the present work.

The dramatic improvement in saturates-aromatics separation upon decreasing the oven temperature is shown for an actual sample by the chromatograms in Figure 1. The sharp initial eluting peak is due to the saturates. At 35°C there is almost baseline separation between the saturates and the monoaromatic group of peaks. An added advantage of operating at the lower temperature is the shorter retention times, which would result in shorter analysis times per sample. For example, phenanthrene elutes in 11 min. at 90°C compared to 6 min. at 35°C This can be attributed to increased density of the supercritical CO_2 at the lower temperature, which increases its solvating ability (8).

B. Effect of Pressure: Data are not shown, but there was some improvement in separation between saturates and aromatics at 90°C when the pressure was increased from 3250 to 3600 psi, presumably due to the increased density of the CO_2. At 35°C, however, there was virtually no change in the separation over the pressure range of 3000 and 4200 psi.

C. Effect of Stationary Phase: Grizzle and Sablotny (12) employed HPLC with two aminosilane columns in series and hexane/methylene chloride as the mobile phase to separate saturates and aromatics. Lundanes and Greibrokk (13) reported that a silver-impregnated silica column was required to obtain complete separation of saturates and aromatics by SFC using CO_2. Based on these studies we investigated three other columns or combinations in an attempt to improve upon the separation between saturates and aromatics. The data obtained at a pressure of 3600 psi and temperature of 35°C are shown in

Table 1. It can be seen that the separation using the silica/cyano (Si/CN) combination is not as good as that of the silica at the same temperature. C_{30} and xylene have the same k value using the Si/CN, whereas C_{30} has a smaller k value than xylene with the silica alone. For the amino (NH_2) column the separation between saturates and aromatics is much poorer; in this case C_{30} has the same k value as hexamethylbenzene. From the limited number of compounds run, it appears that the series combination of silica/20% $AgNO_3$ on silica (Si/Ag) is no better than silica at 90°C. It is concluded that of the stationary phases studied in our SFC system, the best saturates-aromatics separation is obtained using a 5μ silica column.

Calibration

In order to check FID response factors for saturates and aromatics, some calibration studies were carried out. The calibration curves were determined using saturates and aromatics fractions prepared from four middle distillate samples using the procedure reported by Sawatzky et al (11). Recoveries of material from the column ranged from 81 to 99 wt%, indicating the loss of some lower boiling components. The SFC chromatograms of one of the samples and of its separate fractions using the silica column at a pressure of 3250 psi and temperature of 90°C, are shown in Figure 2. The relatively high degree of purity of each fraction implies that the separations by column chromatography and SFC are similar making the fractions suitable for calibration purposes.

The calibration curves obtained over a broad range of concentration using CS_2 solutions of the saturates and aromatics fractions are shown in Figure 3. The data points were fitted to the line: $y = A*x$. The response factors as given by the slopes of each line differ by only 5%. Differences of this order of magnitude were reported for GC/FID work on model compounds (14), from which it was concluded the response factors are more or less eqivalent.

Curvature was noted in the saturates response above approximately $100x10^6$ area counts, whereas the aromatics response was linear to $300x10^6$ area counts. The likely reason for this behavior is that the FID becomes saturated above a certain concentration. The saturates, which have a much sharper peak, saturate the detector at a lower sample size than do the aromatics. Because of this non-linear behavior, it was necessary to reduce the concentration of sample reaching the FID by dilution. CS_2 was chosen as the solvent because of its low FID response. It was found for all samples in this study that dilution by a factor of ten was sufficient to bring the saturates into the linear range.

Because of the close agreement between saturates and aromatics response for fractions obtained from actual samples, it was decided that the integrated area percentages may be used directly to quantitate saturates and aromatics provided that samples are diluted such that the components are within the linear range of the detector and that a small correction is made for the area of the impurity peak from the CS_2.

Repeatability and Accuracy

The wt% aromatics values were obtained from analyses of duplicate (1:10) dilutions in CS_2 of each of 22 samples of heating oils and diesel fuels. Standard deviations ranged from 0 to 1.4 wt%. A pooled standard deviation value of 0.4 wt% was caluculated from all data using the formula given by Snedecor and Cochran (15). According to ASTM C 670-81 (16) the standard deviation is multiplied by the factor 2.83 to obtain a repeatability. For the present data this repeatability statement is as follows: "Duplicate measurements by the same operator should be considered

suspect if they differ by more than 1.1 wt% 19 times out of 20". This repeatability compares favorably with that reported for the FIA method (1).

These particular repeatability measurements were carried out by a chemical technologist with one year of gas chromatographic experience. Three days were required for this individual to become familiar with the operation of the instrument and to perform the analyses. This indicates the relative simplicity of the technique, and suggests its suitability for use in refinery control laboratories.

The accuracy of the method could not be determined using actual samples since the absolute aromatics contents were not known. An indication of the accuracy, however, was made using known mixtures of hexadecane and naphthalene in CS_2. The differences between actual and measured values ranged from 0 to 1 wt%.

Comparison to the FIA Method

Despite its disadvantages, FIA is the most widely used standard method in the oil industry for aromatics determination. For this reason it was used as a basis for comparison of the present SFC/FID results. This comparison is shown by the plot in Figure 4. A linear regression of the data, indicated by the solid line in Figure 4, yielded a correlation coefficient of 0.9018. The 95% confidence interval for this regression is given by the dashed curves. The consistent bias of all but three of the points to higher values by SFC/FID (slope=0.97) probably reflects the fact that the output of FIA is in vol% whereas that for SFC/FID is in wt%. This has also been indicated in the work of Norris and Rawdon (2).

There are two possible explanations for the three samples whose points lie outside the confidence limits. First, these samples yielded olefins values by FIA greater than 3 vol%. High concentration of olefins do interfere with the separation between saturates and aromatics on a silica column (17), which might result in the lower aromatics values by SFC. Secondly, two of these three samples contain components boiling well above 315°C which makes the FIA results questionable for these samples.

Classification of Aromatics by Number of Rings

The capacity factor data for the silica column at both 90 and 35°C shown in Table 1 in general indicate a grouping of the aromatics according to number of rings. The only significant overlap occurs between the monoaromatics, hexamethylbenzene and octahydroanthracene, and the diaromatic compounds. It is suspected that these monoaromatics overlap because of the large amount of pi electron delocalization over the ring structures. For the model compounds considered in the present work good separation is obtained between the diaromatics and polyaromatics.

Stationary phases other than silica, such as amino-modified silica, have been employed to separate polycyclic aromatic hydrocarbons by HPLC (12,19) and by SFC (20). Our SFC data using a series combination of Si/CN stationary phases, shown in Table 1, indicate marginally better separation between mono- and diaromatics compared to silica alone, but poorer saturates-monoaromatics separation. The NH_2 column provides the best separation between mono- and diaromatics, but very poor saturates-monoaromatics separation (the k value for C_{30} is greater than most of the monoaromatic compounds as seen from Table 1). Finally, with the series combination of Si/Ag, the separation among aromatic types appears to be no better than the silica column. It is concluded that, of the stationary phases studied in the present work, a single silica column would be the one preferred for quantitation of aromatics according to number of rings.

CONCLUSIONS

A method employing SFC with FID, similar to that reported by Norris and Rawdon for the analysis of gasolines (2), has been developed for the determination of aromatics in middle distillate fuels. The method is simple, employs relatively inexpensive equipment, gives good repeatability and provides results which correlate well with those obtained by FIA. The SFC method is not affected by sample color, appears to be applicable to samples with final boiling points as high as 450°C and should be suitable for use in a refinery control laboratory. Initial indications are that the determination of aromatics according to the number of rings can be accomplished by SFC/FID.

ACKNOWLEDGEMENTS

The authors would like to thank J. Steppler and R. Dietrich of Chemex Labs (Alberta) Ltd., Calgary, AB, Canada for their assistance in this work.

REFERENCES

1. "Manual on Hydrocarbon Analysis", 3rd Edition, American Society for Testing and Materials, D 1319, Philadelphia, PA, 1977.
2. T.A. Norris and M.G. Rawdon, Anal. Chem., 56, 1767 (1984).
3. J.C. Suatoni and R.E. Swab, J. Chromatogr. Sci., 13, 361 (1975).
4. T.V. Alfredson, J. Chromatogr., 218, 715 (1981).
5. D.J. Cookson, C.J. Rix, I.M. Shaw and B.E. Smith, J. Chromatogr., 312, 237 (1984).
6. P.C. Hayes and S.D. Anderson, Anal. Chem., 57, 2094 (1985).
7. H.E. Schwartz and R.G. Brownlee, J. Chromatogr., 353, 77 (1986).
8. P.A. Peaden and M.L. Lee, J. Liq. Chromatogr., 5(Suppl. 2), 179 (1982).
9. M. Novotny, J. High Resol. Chromatogr. & Chromatogr. Comm., 9, 137 (1986).
10. H.E. Schwartz, J.W. Higgins and R.G. Brownlee, LC-GC, 4, 639 (1986).
11. H. Sawatzky, A.E. George, G.T. Smiley and D.S. Montgomery, Fuel, 55, 16 (1976).
12. P.L. Grizzle and D.M. Sablotny, Anal. Chem, 58, 2389 (1986).
13. E. Lundanes and T. Greibrokk, J. Chromatogr., 349, 439 (1985).
14. W.A. Deitz, J. of Gas Chromatography, 68, February, 1967.
15. G.W. Snedecor and W.G. Cochran, "Statistical Methods", Seventh Edition, Iowa State University Press, Ames, IO, p.91, 1980.
16. "Preparing Precision Statements for Test Methods for Construction Materials", C 670-81, Annual Book of ASTM Standards, 1984.
17. B.J. Fuhr and L.R.Holloway, Alberta Research Council, Edmonton, Alberta, unpublished data.
18. P.J. King and A. Sagarra, in "Modern Petroleum Technology", G.D. Hobson and W. Phol, Eds., 4th Ed., Institute of Petroleum, Applied Science Publication Service, 1973.
19. S.A. Wise, S.N. Chesler, H.S. Hertz, L.R. Hilpert and W.E. May, Anal. Chem., 49, 2306 (1977).
20. R.M. Campbell and M.L. Lee, Anal. Chem., 58, 2247 (1986).

TABLE 1

Comparison of Capacity Factors of Some Model Compounds Using Different Stationary Phases*

Compound	Silica 90°C	Silica 35°C	Si/CN 35°C	NH_2 35°C	Si/Ag 35°C
Saturates:					
N-pentane	-	-	-	-	0.00
N-hexane	0.00	-	-	-	-
3-Methylheptane	0.02	-	-	-	-
N-decane	0.04	0.00	-	-	-
Cyclohexane	0.04	-	-	-	-
Dimethylcyclohexane	0.05	0.04	-	0.00	-
Hexadecane	0.11	-	-	-	-
Decalin	0.13	0.05	-	-	-
Eicosane (C_{20})	0.18	0.04	-	-	0.17
Triacontane (C_{30})	-	0.09	0.15	1.12	0.26
Monoaromatics:					
Benzene	0.16	0.17	-	-	-
Toluene	0.19	0.17	-	-	-
3-Ethyltoluene	0.24	0.16	-	-	-
O-xylene	0.26	0.20	0.15	0.27	0.26
Indane	0.33	0.25	-	-	-
1-Phenydecane	0.39	0.24	-	-	-
Tetralin	0.41	-	0.27	0.62	-
Hexamethylbenzene	0.69	-	0.47	1.12	-
Octahydroanthracene	0.80	-	0.54	1.62	-
Diaromatics:					
Naphthalene	0.53	0.37	0.41	1.12	0.49
2-Methylnaphthalene	0.56	-	0.47	1.27	-
Thianaphthalene	0.56	-	0.47	1.27	-
Biphenyl	0.70	-	0.44	1.46	-
Acenaphthalene	0.80	-	0.65	-	-
Bibenzyl	0.92	-	0.57	-	-
Polyaromatics:					
Fluorene	1.02	-	-	-	-
Dibenzothiophene	1.16	-	-	-	-
Anthracene	1.22	-	-	-	-
Phenanthrene	1.27	0.85	1.15	4.85	1.08
Thianthrene	1.76	-	-	-	-
Fluoranthene	1.82	-	1.78	-	-
Pyrene	1.92	-	-	-	-
Chrysene	-	1.89	-	-	-

* All runs were carried out at a pressure of 3600 psi.

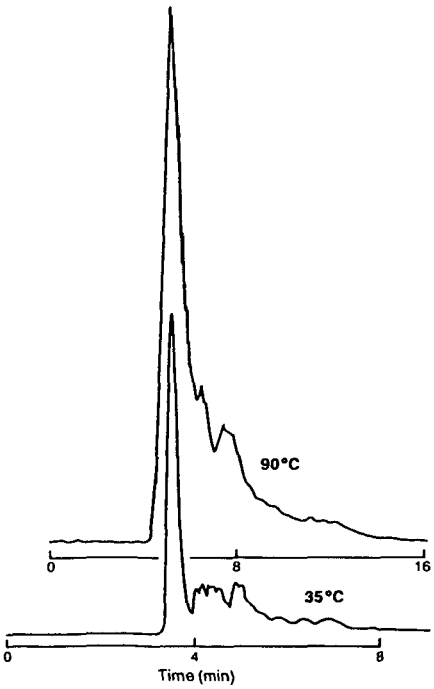

FIGURE 1: SFC chromatograms of a middle distillate sample at temperatures of 90 and 35 °C using a silica column and pressure of 3600 psi.

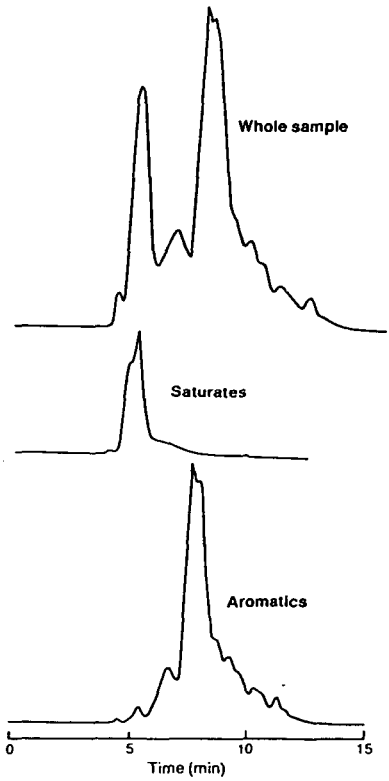

FIGURE 2: SFC chromatograms obtained at 90°C and 3250 psi of a whole middle distillate sample and of its saturates and aromatics fractions separated by column chromatography.

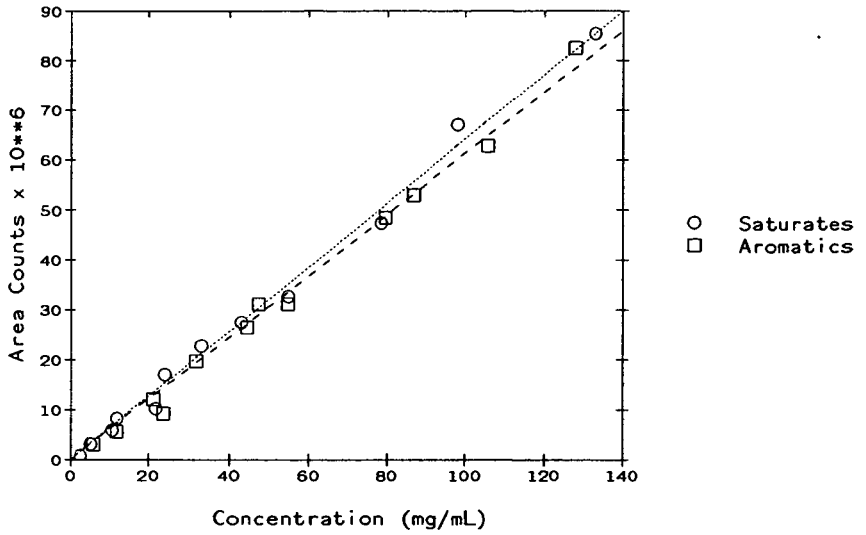

FIGURE 3: SFC calibration curves using saturates and aromatics fractions separated from middle distillates by column chromatography.

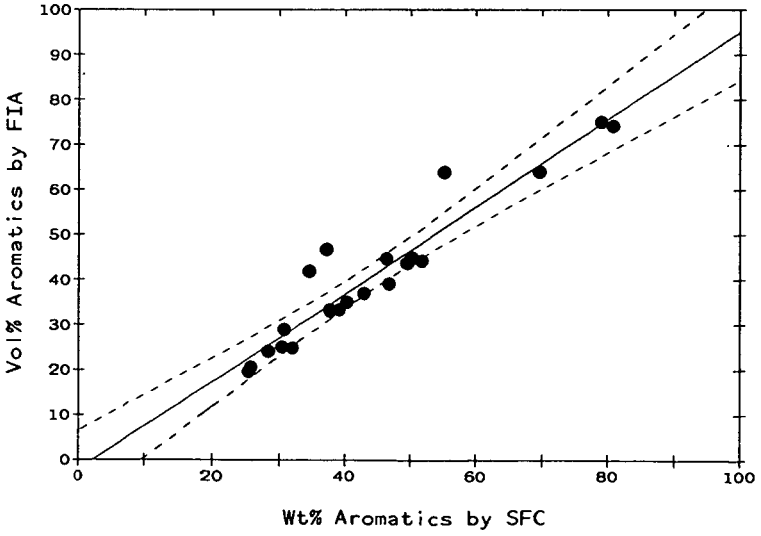

FIGURE 4: Comparison of aromatics content of middle distillates by SFC and FIA.

THE DEPOLYMERIZATION OF A MODEL COAL POLYMER

I. Lee, C. M. Sliepcevich and R. G. Mallinson

School of Chemical Engineering and Materials Science
University of Oklahoma
Norman, Oklahoma 73019

INTRODUCTION

While the macromolecular nature of the organic matter of coal has been known for some time (1), the manner in which the organic structure is held together has been a focus for a much shorter time and is still the subject of considerable scrutiny (2,3,4). It has been established that the macromolecular crosslinked structure of coal is the primary reason for its insolubility, but swellability, in organic solvents. The nature of the crosslinks, whether of a covalent or lesser type, is not really in dispute, but, rather, the relative amounts and importance of the probable interactions. The difficulties in establishing a clear concept no doubt lie in the very heterogeneous nature of coal, including the presence of trapped or "guest" molecules, and the diversity of coals of widely varying origins and ages.

The most successful approach in attempting to understand the macromolecular structure of coal has been the application of techniques and models from the field of polymer science in considering coals as crosslinked polymer networks (3,4). The difficulties of adapting a theoretical approach for ideal systems to such a heterogeneous, non-ideal, system as coal, have recently been pointed out (5,6). Nevertheless, for a pure polymer system used as a model for coal, the results should provide helpful insights into the nature of the thermal degradation of crosslinked polymer networks and coals.

In this work, a model coal polymer network has been synthesized under conditions of thermal liquefaction. The degradation of the macromolecular network and production of soluble products are followed as a function of reaction time.

EXPERIMENTAL

A crosslinked polymer network was produced using the difunctional monomers a,a'-dichloroxylene and hydroquinone with trihydroxy benzene as the trifunctional crosslinking agent. The polymer which was desired was a crosslinked aromatic based polymer in which all of the linkages, including the crosslinks, were relatively thermally labile. Thus, the linkages produced in the condensation polymerization of these monomers should all be of the benzyl phenyl ether type, which cleave readily at 350 ° C to produce phenolic hydroxyl and aromatic methyl groups when tetralin is used as a solvent (7). Figure 1 shows the monomer structures and the steps in the production of the polymer. The hydroxyl monomers were converted to their sodium salts and dissolved in water, while the dichloride was dissolved in acetone. These were then mixed and refluxed at atmospheric pressure for four hours to produce an insoluble product. The polymer which was produced was insoluble in all solvents tested, including THF and pyridine. Analysis of the polymer included carbon, hydrogen, oxygen, sodium and chlorine elemental analyses which were carried out by Huffman Laboratories, and swelling analysis. Swelling analyses were carried out in pyridine using the procedure of Larsen et al. (8).

Once the polymer had been synthesized, degradation experiments were carried out in a microtubing bomb type reactor. Approximately 0.5 grams of polymer, accurately weighed, was put into the reactor with 2.0 grams of tetralin. The reactor was then sealed and pressurized with nitrogen gas to 1000 psig. The reactor was immersed in a fluidized bed sandbath maintained at 350 ± 5 ° C. The internal reactor temperature reached the steady state temperature within one minute and, at the end of the desired reaction time, was removed from the bath and quenched in water for an essentially

instantaneous cool down.

The reactor contents were then removed and a soxhlet extraction with THF was carried out to separate soluble and insoluble materials. The THF (and tetralin) was removed from the soluble fraction by rotary evaporator and the THF removed from the insoluble matter in a vacuum oven. Both fractions were weighed and the material balance could be closed to within five percent with a few exceptions which were within ten percent. The insoluble material was then subjected to swelling analysis and hydroxyl group analysis using the acetylation technique following the procedure of Cronauer et al. (9). The soluble material was analyzed by gel permeation chromatography.

RESULTS

As mentioned above, it was initially intended that all linkages in the polymer would be of the benzyl phenyl ether type. However, the degradation results showed that after significant conversion of the initial insoluble polymer to soluble products at short reaction times, an asymptotic limit of about 40 percent was reached after which no increase in conversion was observed, as can be seen in Figure 2. After examining the elemental analysis data and the organic chemistry literature, it appeared that a side reaction involving nucleophilic attack of the aromatic rings by the hydroxyl groups was possible. This reaction altered the structure of the polymer by including diphenyl ether type structures, which are considerably more refractory than the benzyl phenyl ethers (7). This additional structure is illustrated in Figure 3 by the symbol, T. With this knowledge, the polymer structure could be broken down into the groups shown in Figure 3 for purposes of analysis. A sample of the polymer structure is shown in Figure 4 with the different structural groups outlined. The quantities of all of these groups could be determined by their algebraic relationships with the elemental analyses, including the end group analysis provided by the sodium and chlorine analyses. The reduction of the structure into groups allowed the determination of the quantities and types of crosslinks present in the polymer structure. This knowledge about the crosslinks, with the use of a modified Flory-Rehner (10,3,4) theory, provides detailed information about the network. The molecular weight between crosslinks as well as the size of the "loops" in the network may be determined.

With the appropriate parameters, the initial molecular weight between crosslinks is calculated to be 600 for the observed swelling ratio of 1.34. The interaction parameter, χ, was determined from the correlation of Lucht (11) based solely on the carbon content of the material, which was developed for coals. This parameter is currently being determined experimentally for this system. Upon degradation, the swelling behavior follows the conversion results in that the ratio increases dramatically within the first four minutes, and then levels off to an asymptotic limit of about 1.8, as may be seen in Figure 5. From the modified Flory-Rehner theory, a molecular weight between crosslinks of 900 is calculated. The behavior of both the conversion and molecular weight between crosslinks is qualitatively quite similar to what one might expect of a coal at this temperature. It follows that the more thermally labile crosslinks have been cleaved and then stabilized by the donor solvent, causing a significant amount of soluble material to be produced. At the same time the network opens up, but there remains a substantial amount of insoluble material due to the stability of the more refractory crosslinks. Figure 6 shows the hydroxyl group concentration of the polymer as a function of reaction time with the results as expected for the cleavage of the benzyl phenyl ether linkages at the conversions observed.

The soluble materials produced show a range of molecular weights from below 300 up to about 1000. Calibration of the GPC was accomplished with model compounds having molecular weights up to 532, so the values above that could have some absolute error from the extrapolation. Figure 7 shows the evolution of the molecular weight distribution with reaction time. The data are normalized per gram of initial polymer used so that the area under the curve is proportional to the mass of soluble material produced and becomes larger with higher conversions at longer reaction times. As may be seen, the general trend is for increased material of all molecular weights to be produced as the reaction

time and conversion increases. However, the lower molecular weight material, below about 300 tends to increase more rapidly than the bulk of the curve, which may be indicative of continued depolymerization within the material which has already become soluble. Also, at the higher molecular weights, above about 700, the increase is also larger than for the bulk of the curve, with a pronounced peak developing for the two longest reaction times shown. It may be that as more crosslinks are broken, larger "pieces" of structures become soluble because of increases in the numbers of hydroxyl and methyl groups per "molecular piece", which aid the solubility of such "pieces".

SUMMARY

In summary, the goal of this work has been to develop a synthetic macromolecular network which may be used as a model for coal networks, and to take advantage of the high degree of characterization available such that the network may be thermally degraded and nsights into the degradation of the networks in coal may be gained. Also, with the increased use of thermosetting polymer networks for materials applications, this knowledge is applicable to the understanding of thermal (or random) degradation and stability of these systems. This experimental work is being conducted in parallel with a modeling effort for the degradation of polymer networks.

ACKNOWLEDGEMENTS

This work was supported by the Energy Resources Institute and Oklahoma Mining and Minerals Resources Research Institute of the University of Oklahoma and in part by the U. S. Department of Energy under grant No. DE-FG01-87FE1146.

REFERENCES

(1) Van Krevelen, D. W.; *Fuel*, **44**, 229 (1965).

(2) Sanada, Y. and Honda, H.; *Fuel*, **45**, 295 (1966).

(3) Larsen, J. W. and J. Kovac; *Organic Chemistry of coal*, ACS Symposium Series 71, Chapter 2, American Chemical Society, Washington DC (1978).

(4) Lucht, L. M. and N. A. Peppas; in *Chemistry and Physics of Coal Utilization*, B. R. Cooper and L. Petrakis, Eds.; Am. Inst. Physics, New York (1981).

(5) Hsieh, S. T. and J. L. Duda; *Fuel*, **66**, 170 (1987).

(6) Painter, P., J. Nowak, M. Sobkowiak and J. Youtcheff; *ACS Fuel Chem. Div. Preprints*, **32**, #1, 576 (1987).

(7) Wooding, G. W.; M.S. Thesis, Purdue University (1982).

(8) Larsen, J. W., T. K. Green and J. Kovac; *Fuel*, **63**, 935 (1984).

(9) Cronauer, D. C. and Ruberto, R. G.; EPRI Report Number AF-442 (1977).

(10) Lee, I.; M.S. Thesis, University of Oklahoma (1986).

(11) Flory, P. J. and J. Rehner; *J. Chem. Phys.*, **11**, 521 (1943).

(12) Lucht, L. M.; Ph. D. Thesis, Purdue University (1984).

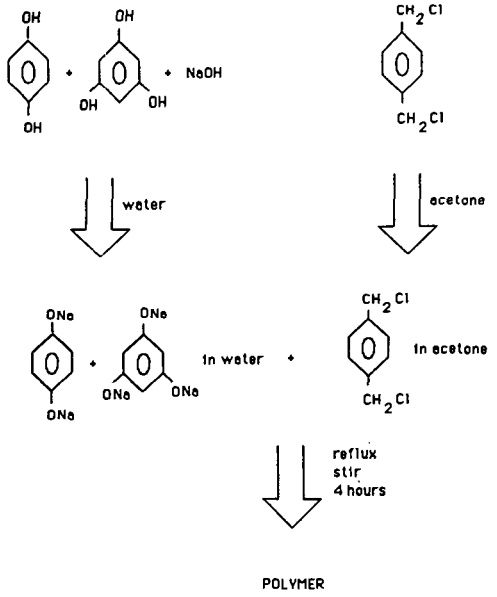

Figure 1. Preparation of the Crosslinked Polymer.

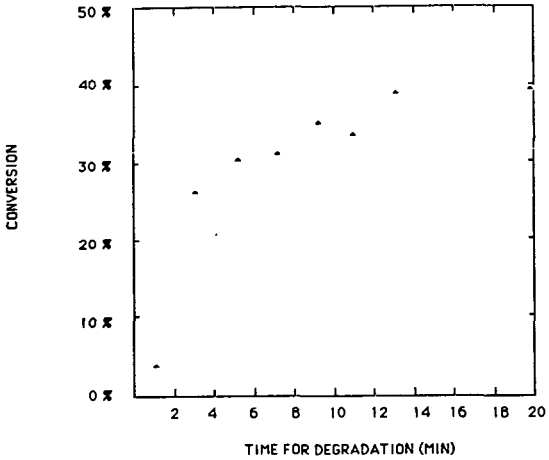

Figure 2. Conversion of the Polymer Network to Soluble Products.

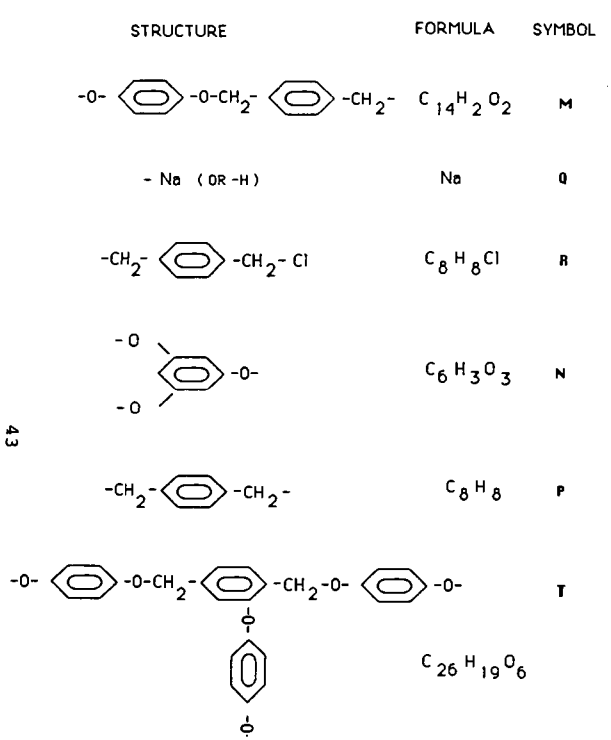

Figure 3. Basic Structural Units of the Polymer Network.

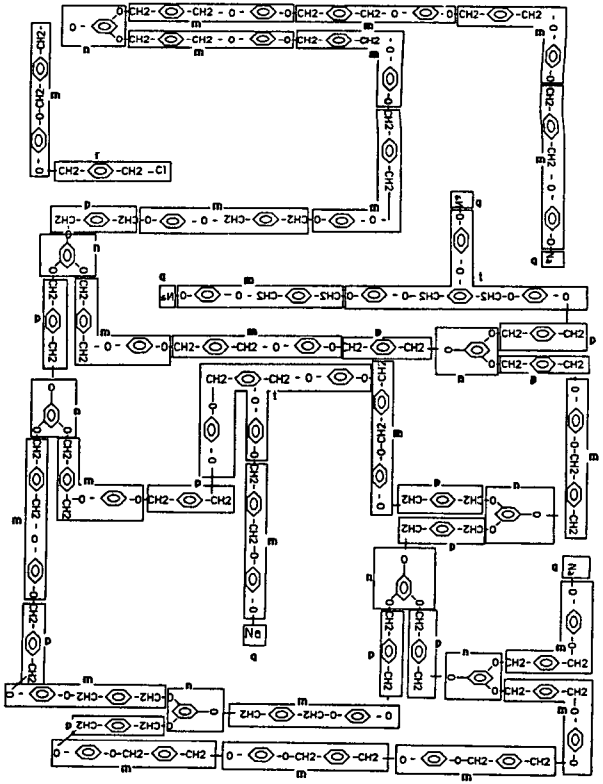

Figure 4. The Polymer Network.

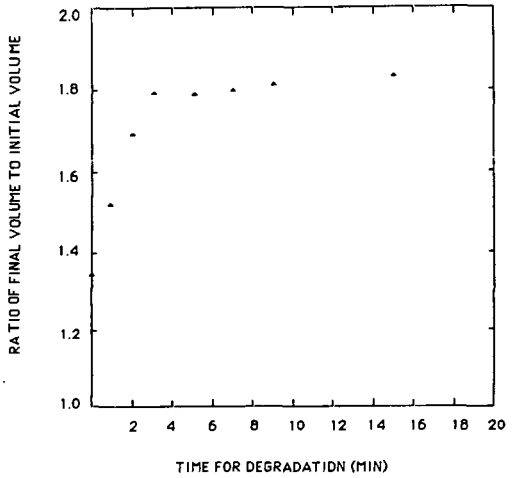

Figure 5. Swelling Ratio of the Network as a Function of Reaction Time.

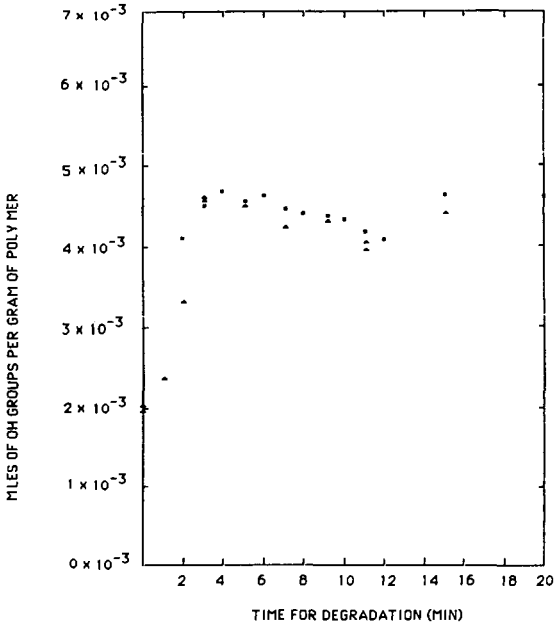

Figure 6. Hydroxyl Group Content of the Degraded Polymer.

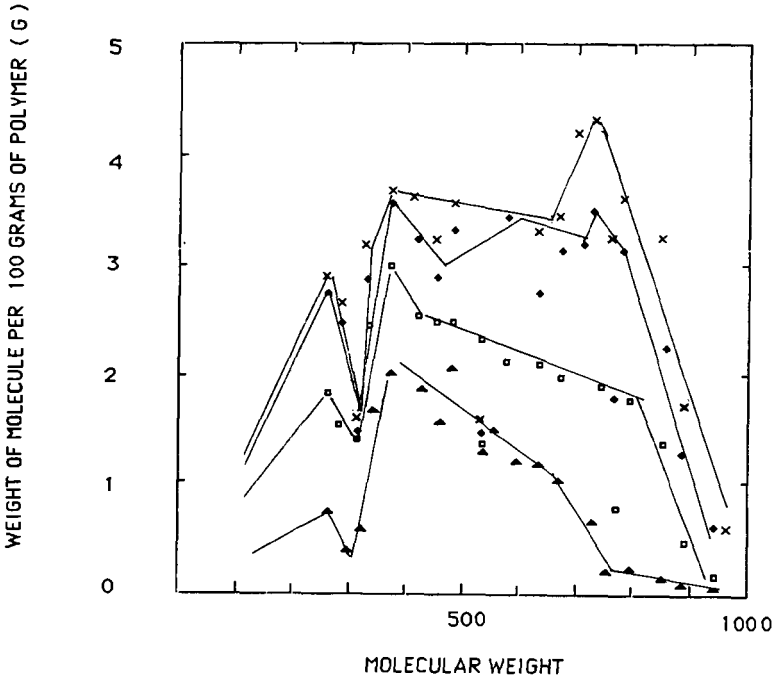

Figure 7. Molecular Weight Distributions of the Soluble Products.

Fused Salt Reactions of Organosulfur Compounds

Michael A. Nowak, Bruce R. Utz, Daniel J. Fauth
and Sidney Friedman

U.S. Department of Energy
Pittsburgh Energy Technology Center
P.O. Box 10940
Pittsburgh, PA 15236

INTRODUCTION

The treatment of coal with molten caustic is an effective method for cleaning coal (1). Molten caustic treatment removes not only mineral matter but most of the sulfur, including organic sulfur, from coal. While the chemical processes leading to the removal of inorganic sulfur have been examined (2), the mechanism of organic sulfur removal is less understood. Coal characterization studies suggest that the organosulfur moieties in coal may be largely thiophene-type ring structures (3-5). A preliminary investigation in this laboratory studied the reaction of benzothiophene with sodium and potassium hydroxides (6). Evidence was obtained that o-thiocresolates were intermediates in the desulfurization reaction (Equation 1). The overall reaction is multistep; the ring opening is a key step, since only after conversion to a thiol derivative does desulfurization take place. Our findings on the desulfurization of thiols and thiol derivatives will be discussed here.

EXPERIMENTAL

All reagents were used as purchased from commercially available sources except the thiolate salts, which were prepared as previously described (6). Potassium hydroxide contained approximately 10-12 percent moisture, and all other salts were anhydrous. An "inert fused salt diluent" (IFSD), consisting of a 36:55:9 KCl:LiCl:NaCl mixture by mole percent, was also used and had a eutectic point of 346°C. The hydroxide mixture used was a 60:40 KOH:NaOH mixture by weight (50:50 molar).

Reactions were conducted in commercially available 1/2-inch tubing unions fabricated from corrosion resistant Monel, Inconel, or Carpenter-20 alloys. Before use, the unions were washed with tetrahydrofuran and methylene chloride in order to remove any oils. One end cap was placed on the union and tightened to 30 ft lb. The half-assembled reactor was transferred into a nitrogen-purged glove box, where it was charged with approximately 0.40 gram of the organic compound and, when necessary, 2.40 grams of the powdered hydroxide(s) or salt mixture. The second end cap was placed on the reactor. After removing the reactor from the glove box, the second end cap was tightened to 30 ft lb.

The reactor was bolted in a bracket assembly and immersed in a fluidized sand bath that was preheated to the reaction temperature. For most experiments, mixing was effected by shaking the reactor assembly using a mechanical wrist action shaker. Shaking the reaction vessel had little effect on product distribution. After the specified reaction time, the reactor was cooled rapidly by immersion in tap water. The reactor was opened while submersed in 50 mL methylene chloride to dissolve volatile and neutral organic materials.

Glass reactors were prepared by sealing one end of a six-inch length of heavy-walled Pyrex tubing (12.7-mm-o.d. x 2.4-mm-i.d.). The tube was placed in the glove box and charged with approximately 0.10 gram of organic compound and, where appropriate, 0.40 gram of hydroxide(s) or salt mixture. The tube was

removed from the glove box, freeze-thaw degassed, and sealed under vacuum while the lower portion of the tube remained frozen in liquid nitrogen. After warming to room temperature, the ampoule was loaded into a 3/4-inch stainless steel reactor tee assembly (7) and pressurized to equalize the pressure buildup anticipated within the glass ampoule at reaction temperatures. The tee assembly was then submersed in a preheated fluidized sand bath for the appropriate reaction time, removed from the sand bath, and allowed to cool slowly to room temperature. The pressure was vented from the tee assembly, and the ampoule removed. The ampoule was scored and cracked open while submersed in 50 mL methylene chloride.

The methylene chloride washings were transferred into a flask containing 1,2,4,5-tetramethylbenzene as an internal standard for GLC analysis. If the reactor contained salts, it was then shaken with 50 mL distilled water containing sufficient concentrated HCl to adjust the acidity of the final solution to pH 3. The time required to dissolve the salts completely was generally 10-30 minutes. The aqueous solution was decanted into a separatory funnel, where it was extracted with two 25-mL portions of methylene chloride. The methylene chloride extracts were added to a flask containing an internal standard. Aliquots of the methylene chloride solutions were analyzed by GLC. Products were further characterized by GC/MS. Where necessary, solutions were subjected to pressure filtration through microporous membranes to remove insoluble materials (8). The presence of methylene chloride soluble polymers was determined by careful removal of solvent and volatile materials in vacuo and weighing the residues.

RESULTS AND DISCUSSION

The thermal chemistry of alkyl thiolate salts was first examined at the turn of the century (9), and since then little has been done to reveal the mechanisms of their decompositions. Most studies involved aliphatic thiolates, and only recently has anyone examined alkali metal thiolates (10,11). In general, thiolate salts are known to undergo only one pyrolysis reaction: decomposition at or near their melting point to give an organic sulfide and a metal sulfide (Equation 2).

We chose as our model compounds derivatives of the simplest aromatic thiol, thiophenol. Potassium thiophenolate or sodium thiophenolate were heated at 375°C for thirty minutes in a metal union in the presence of potassium hydroxide, sodium hydroxide, or a mixture of sodium and potassium hydroxides, or the IFSD, or as neat samples. The IFSD is molten at 375°C and was used to simulate the ionic character of the molten hydroxide media while being chemically inert towards organosulfur compounds under these conditions. By comparing the chemistry of thiophenolates in molten caustic, or IFSD, or as neat samples, we hoped to determine whether the caustic reacted with thiolate to produce a sulfur moiety more amenable to desulfurization, thus facilitating bond breaking.

We have found that, in the absence of a catalyst, neat potassium and sodium thiophenolates are stable at 375°C for extended periods of time. When potassium thiophenolate or sodium thiophenolate was treated with a molten 60:40 KOH:NaOH mixture in a corrosion-resistant union (Equation 3), a number of reaction and decomposition products were observed. Some starting material was recovered as thiophenol, and small quantities of phenyl sulfide were obtained. Significant quantities of the desulfurization product, benzene, were observed, but also some biphenyl was obtained. A number of minor products (accounting for less than 28% of the material recovered) were also observed. Methylene chloride insoluble materials that appeared as black solids were sometimes observed. Reactions conducted in the presence of hydrogen led to increased yields of benzene and lower yields of black solids (6). These observations lead us to believe that phenyl radicals are intermediates in these reactions, and that the black solids were being formed by uncontrolled polymerization of some radical species. In some cases, some methylene chloride soluble materials had insufficient volatility to be observed by GLC. These were assumed to be oligomeric materials. Products con-

taining hydroxyl groups (phenol) or several sulfhydryl groups were sometimes observed, but generally these products were insignificant. The yields of desulfurized product from the reaction of sodium thiophenolate in sodium hydroxide or potassium hydroxide (12%-16%) were lower than the yields from the reaction of potassium thiophenolate in sodium or potassium hydroxide (30%-40%).

When reactions were conducted in the same reactors using IFSD as a reaction medium, a significant difference in the chemistry of sodium thiophenolate versus potassium thiophenolate was observed. In the IFSD, diaryl sulfide formation competes with desulfurization. Phenyl sulfide was the only product observed when sodium thiophenolate decomposed in IFSD. Potassium thiophenolate decomposed in IFSD to produce the desulfurized product benzene, although a small amount of phenyl sulfide was also produced.

During the course of these studies, inconsistent results led us to observe carefully the product distributions in the different reactor vessels. Potassium thiophenolate was heated at 375°C for 30 minutes as a neat sample or in IFSD using new, "pristine" reactors. When these reactions were conducted in pristine Inconel or Carpenter-20 reactors, no desulfurization took place (Equation 4). Desulfurization was observed in experiments conducted in pristine Monel reactors. The reactors were then pretreated with molten caustic. Potassium thiophenolate was then reacted in these same reactors, and desulfurization products were observed in all cases (Equation 5). No significant increase in desulfurization was observed in experiments conducted in pretreated Monel reactors. Clearly, the metal walls of these reactors were acting as catalysts in the desulfurization mechanism or as reactants that were causing desulfurization. For Inconel and Carpenter-20 alloys, molten caustic was necessary to "activate" the metal surface.

In order to examine the catalytic effect of the metal species in these reactors, a limited systematic study was undertaken. The alloys from which these reactors were fabricated consists mainly of nickel, with individual alloys containing significant quantities of iron, copper, or chromium along with traces of manganese and other metals. Reactions were conducted in sealed glass ampoules to observe the chemistry of thiophenolates in the absence of any metals. In subsequent reactions, individual metals were added to see if they effect desulfurization. As expected, potassium thiophenolate is unreactive in the absence of any other reagents. Again, in the presence of IFSD, potassium thiophenolate provides phenyl sulfide as the major product. Some starting material was recovered. Reaction of potassium thiophenolate in the presence of caustic did not lead to desulfurization. In the presence of nickle powder or Monel shavings, with or without fused salts, significant quantities of desulfurization products (benzene and biphenyl) are obtained. Potassium thiophenolate in the presence of IFSD and iron powder does not undergo desulfurization.

In an effort to understand further the carbon-sulfur bond breaking processes, the chemistry of thiophenol and diphenyl disulfide was examined. The pyrolysis of aromatic thiols has not been studied as extensively as that of aliphatic thiols. When aromatic thiols or disulfides are heated, the major products are diaryl sulfides (12). There are several papers that report desulfurization products arising from pyrolysis of thiophenol at very high temperatures (700°C) or pyrolysis over catalysts at moderately high temperatures (300°-580°C) (13-15). Flow pyrolysis of diphenyl disulfide of 400°C yields thiophenol and diphenyl sulfide (16).

Our studies show that at 375°C, in the absence of any catalytic species, thiophenol and diphenyldisulfide decompose to phenyl sulfide. When heated in the presence of an active catalyst (Monel shavings, nickel or copper powder), thiophenol or diphenyl disulfide gives phenyl sulfide as its major product, but desulfurization products (benzene and biphenyl) are also observed.

We have observed that naphthalene thiols undergo desulfurization more readily than thiophenol. This is in agreement with observations reported in the literature (15).

CONCLUSIONS

In the presence of fused salts, an increase in the reactivity of thiolate salts is observed perhaps because the fused salts function as solvents, and increase the probability of bimolecular reactions. Bimolecular reaction giving rise to organosulfur species more resistant to desulfurization compete with desulfurization, but in coal, because of the more rigid organic matrix, it is not likely to be a problem.

Caustic is not necessary for desulfurization of thiol derivatives, although it may enhance it. An increase in desulfurization in the presence of caustic may be due to suppression of competing bimolecular reactions or some chemical process that actually speeds the desulfurization reaction. We do not have sufficient evidence to support these or other possible explanations. The desulfurization of aromatic thiols and their derivatives requires a catalyst. One of the species that catalyze these reactions is nickel, but other metals or alloys may also catalyze the desulfurization. In some cases, molten caustic is required to "activate" the catalyst. Additional studies concerning the nature of this catalysis and other possible catalytic species are under way. The chemistries of different aromatic thiols are similar, but changes in the aromatic structure influence their reactivity.

ACKNOLWEDGMENTS

We gratefully acknowledge the technical assistance of Murphy Keller, Thomas Williams, Anthony Selmeczy, and James Knoer. We also acknowledge the Oak Ridge Associated Universities Research Associate Program in which Michael Nowak, Murphy Keller, and Anthony Selmeczy participated.

DISCLAIMER

Reference in this report to any specific commercial process, product or service is to facilitate understanding and does not necessarily imply its endorsement or favoring by the United States Department of Energy.

REFERENCES

1. Masciantonio, P.X. Fuel 1965, 44, 269.

2. Chiotti, P.; Marusczewski, R. Ind. Eng. Chem., Proc. Des. Dev. 1985, 24 (4), 1137.

3. Attar, A. "An Analytical Method for the Evaluation of Sulfur Functionalities in American Coals," DOE Final Report DOE/PC/30145-T1 (DE 84007770) 1984.

4. Spiro, C.L.; Wong, J.; Lytle, F.W.; Greegor, R.B.; Maylotte, D.H.; Lamson, S.H. Science 1984, 226, 48.

5. LaCount, R.B.; Anderson, R.R.; Friedman, S.; Blaustein, B.D. Am. Chem. Soc. Div. Fuel Chem. Preprint 1986, 31(1), 70.

6. Utz, B.R.; Friedman, S.; Soboczenski, S.K. In ACS Symposium Series No. 319, "Fossil Fuels Utilization: Environmental Concerns;" Markuszewski, R., and Blaustein, B.D., Eds.; American Chemical Society: Washington, DC, 1986; Chapter 5.

7. Utz, B.R.; Appell, H.R.; Blaustein, B.D. Fuel 1986, 65, 1085.

8. Utz, B.R.; Appell, H.R.; Blaustein, B.D. Fuel 1986, 63, 1671.

9. Challenger, F. "Aspects of the Organic Chemistry of Sulfur," Butterworths Scientific, London, 1959.

10. Peach, M.E. J. Inorg. Nucl. Chem. 1979, 41, 1392.

11. Peach, M.E. J. Inorg. Nucl. Chem. 1973, 35, 1046.

12. Shagun, L.G.; Papernaya, L.K.; Deryagina, E.N.; Voronkov, M.G. Izv. Akad. Nauk SSSR, Ser. Khim. 1979, (10), 2390.

13. Robertson, H.W.; Steedman, W. Fuel 1966, 45, 375.

14. Johnson, D.E. Fuel 1987, 66, 255.

15. Tits-Skvortsova, I.N.; Danilova, T.A.; Markov, M.A.; Stepanova, I.I.; Osipenko, Ts.D. Khim. Seraorgan. Soedin., Soderzhashch. v Nefteprod., Akad. Nauk SSSR, Bashkirsk. Filial 4 1961, 141. (CA 58:3366).

16. Alnajjar, M.S.; Franz, J.A. Am. Chem. Soc. Div. Fuel Chem. Preprint 1986, 31 (1), 287.

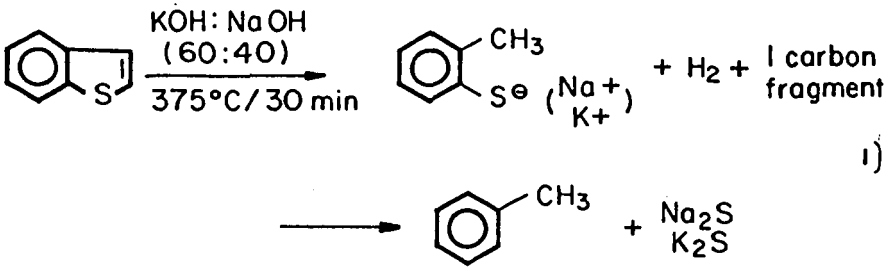
KOH: NaOH
(60:40)
375°C/30 min
CH3
S⊖ (Na+ K+)
+ H2 + I carbon fragment
CH3
+ Na2S K2S

1)

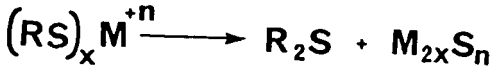
(RS)xM+n
R2S + M2xSn

2)

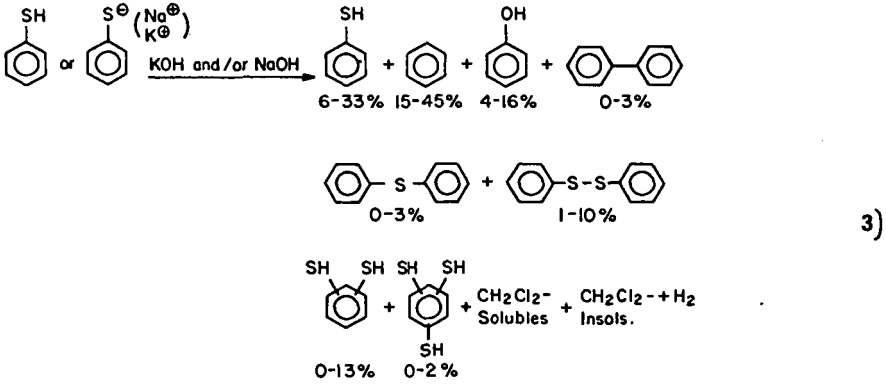
SH
or
S⊖ (Na⊕ K⊕)
KOH and/or NaOH
SH
OH
6-33%
15-45%
4-16%
0-3%
S
0-3%
S-S
1-10%
SH SH SH SH
SH
0-13%
0-2%
CH2Cl2- Solubles
CH2Cl2-+H2 Insols.

3)

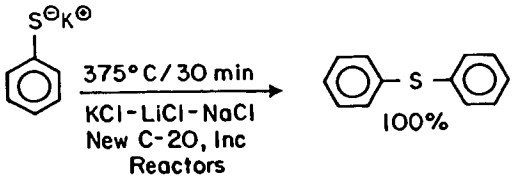
S⊖K⊕
375° C / 30 min
KCl-LiCl-NaCl
New C-20, Inc
Reactors
S
100%

4)

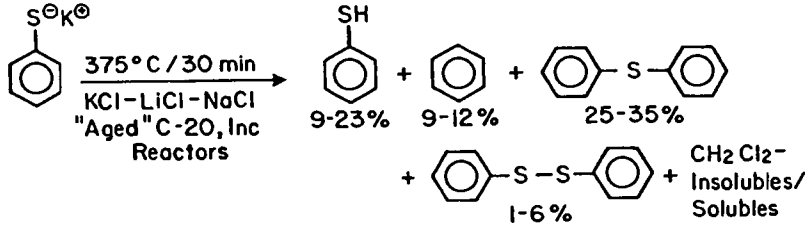
S⊖K⊕
375° C / 30 min
KCl-LiCl-NaCl
"Aged" C-20, Inc
Reactors
SH
9-23%
9-12%
S
25-35%
S
S
1-6%
CH2 Cl2-
Insolubles/
Solubles

5)

EXPERIMENTAL STUDY ON THE FORMATION OF SILICA PARTICLES IN A COUNTERFLOW DIFFUSION FLAME

Shyan-Lung Chung, Huoo-Deng Lin and Chen-Fei Kang

Department of Chemical Engineering
National Cheng Kung University
Tainan, Taiwan, R.O.C.

ABSTRACT

We describe a study on the formation of silica particles in a counterflow diffusion flame. This flame is generated in the impingement region of a fuel (H_2+N_2) and an oxidant (O_2+N_2) gas streams. SiH_4 was used as the precursor for the formation of SiO_2. It was fed into the fuel gas stream. Chemical reaction leading to the formation of SiO_2, nucleation of particles, and their initial growth all occur upstream of the flame. For a sufficiently high temperature flame, aggregates formed upstream fuse to form single, spherical particles as they pass through the flame zone. However, for a low temperature flame, aggregates remain (or partially fuse) as they pass through the flame zone. Samples of particles were collected at the exits of the burner. Particle size, shape, crystalline structure, and chemical composition were analyzed. These results will be presented.

INTRODUCTION

The formation of particles in combustion is a problem of considerable importance in many industrial processes. In coal combustion and gasification processes, formation of particles creates a serious problem of air pollution. On the other hand, formation of particles in combustion flames provides a useful technology for the manufacture of many oxide powders.

In the manufacture of powders using flame technology, the formation of particles involves the following processes: (1) The vapor of the desired material (e.g., SiO_2) is generated in the flame by oxidation of the precursor compounds (e.g., SiH_4) which is fed into the flame. (2) The vapor (in a supersaturated state) nucleates and forms initial particles. (3) The initial particles grow to form the desired powder. Since these processes all occur in the flame, the properties of the powder are greatly influenced by the structure of the flame. The structure of the flame is in term determined by the construction of the burner. The design of the burner is therefore a key element in the flame technology for the synthesis of powders.

In our laboratory, we use the counterflow diffusion flame burner designed by Shyan-Lung Chung and Joseph L. Katz [1,2] to study the formation of SiO_2 particles. A main purpose of the research is to investigate the influence of the burner design and the operating conditions (e.g., temperature, concentration, and gas flow paths) on the properties of the particles.

DESCRIPTION OF EXPERIMENT

A. Burner, Gases and Flame

As shown in Fig. 1, the burner consists of two vertically opposed tubes of rectangular cross section. The oxidant (O_2 diluted with N_2) flows downward from the upper tube, and the fuel (H_2 diluted with N_2)

flows upward from the lower tube. The two gas streams meet near the middle and then flow outward. Each tube contains three channels (separated by 0.08 mm thickness stainless steel plates): a central main channel (12.70 mm × 63.50 mm) and two side channels (12.70 mm × 6.35 mm). Fused silica plates, fitted to the outside of the two side channels, force the combustion gases to flow out along the long sides. Each of the burner tubes was designed to obtain a uniform flow of gas across its mouth by passage of the gases through a perforated plate, a bed of glass beads (1.0 mm diameter), and two stainless steel wire screens. To compensate for heat losses from the sides with fused silica windows, the oxidant and fuel streams in the side channels are enriched in O_2 and H_2, respectively, to precisely the extent required to obtain a temperature distribution which is uniform in the direction normal to the two fused silica windows (i.e., the X-direction; the X, Y, and Z directions are shown in Fig. 1). To prevent deposition of particles on the fused silica windows, no precursor compounds (i.e., SiH_4 in this research) is added to the mixtures which are fed to the side channels. Flanges fitted on each side of the burner openings minimize entrainment of surrounding air and keep the outward gas flow parallel to the burner surfaces. The distance between the two burner mouths is adjustable but has been kept at 15 mm in all the experiments presented here.

The major part of the construction of the burner as described above is the same as that designed by Chung and Katz [1,2]. However, in order to study the formation of particles, we have made some modifications. First, the main channel for the fuel gas stream was divided into three slots in the Y direction using 0.2 mm thickness stainless steel plates. Silane can be added to either the central slot or the side slots to study the effect of different flow paths on the properties of the generated particles. (Note that the dividing plates are removable. In some of the experiments, the undivided channel was used.) Second, nitrogen was added to the combustion gases at the burner exits through ten small holes on each flange. This is both to dilute the particles and to quench the effluent combustion gases so that growth of particles can be ceased at the burner exits where samples of particles are taken.

The N_2, H_2, and O_2 gases used all have the reported purities of 99%. A mixture of 10% semiconductor grade silane and 90% U.H.P. grade H_2 (99.999% purity) was used as the silane source. Each gas flows through a filter (sintered brass filter with 0.5 μm pore size) for the removal of preexisting particles. The gas flow rates were controlled and measured to about 1% accuracy using calibrated rotameters.

The burner produces a flame which is flat, stable, and rectangular in shape [1,2]. Both temperature and concentration distributions are uniform in the horizontal plane (i.e., X-Y plane) [2]. Formation of condensing species (e.g., SiO_2), nucleation of particles and their initial growth all occur upstream of the flame, where the gas flow is almost one-dimensional (i.e., Z direction). These characteristics of the flame offer great advantages for the study of the formation of particles.

B. Temperature Measurement

We used 0.05 mm diameter platinum and platinum -10% rhodium thermocouples to measure temperatures. The thermocouple wires were coated with silica to eliminate catalytic effect. The temperatures thus obtained were corrected for radiation loss.

C. Sampling and Analysis

Particles were collected at the burner exits using glass fiber

filters. The crystalline structure of the powder was examined using an X-ray diffractometer (XRD). The chemical composition was analyzed using an energy dispersive spectrometer (EDS). Particle size and shape were examined using an transmission electron micrograph (TEM). To prepare samples for TEM examinations, particles were dispersed ultrasonically in ethyl alcohol. A drop of this dispersion was placed on the TEM grid, and allowed it to dry.

RESULTS AND DISCUSSION

We describe the results of three experiments in the following. These three experiments were carried out using the same H_2-O_2 flame, i.e., the gas flow rates, and the concentrations of hydrogen and oxygen were all kept constant. The gas flow rates are listed in Table 1. In experiment one, the main channel for the fuel gas stream was not divided. In experiment two and three, this channel was equally divided into three slots. Since the dividing plates are very thin (0.1 mm), their effect on the flame is small.

Table 1.

	Fuel		Oxidizer		
	H_2	N_2	O_2	N_2	
Main channel	2260	1270	1600	1210	(cm^3/min)
Side channel	700	0	525	0	(cm^3/min)

In experiment one, the silane flow rate was 20 cm^3/min, which was equal to 0.56% of the total fuel gases. In experiment two, silane was added only to the two side slots. Its flow rate was 13.3 cm^3/min. In experiment three, silane was added only to the central slot at a flow rate of 6.7 cm^3/min. (Note that the silane concentrations in these two experiments were the same as that used in experiment one, i.e., 0.56% of the fuel gases.) The flow rate of the nitrogen used for quenching at the burner exits was 2200 cm^3/min, which decreased the temperature of the effluent gases by about 200°C.

Because the Pt and Pt-10% Rh thermocouples can not measure temperatures above 2000 K, our temperature measurement was limited to the regions outside the flame zone, where the temperatures were below 2000 K. As mentioned previously, the major construction of the burner is the same as that used by Chung and Katz [1]. The gas flow rates, and the concentrations of hydrogen and oxygen we used were also the same as those reported by Chung and Katz in one of their experiments[1,2]. We compared our thermocouple temperature measurements with theirs and found them to be in excellent agreement. We reproduced their temperature profile and showed it in figure 2.

A. Experiment One

Examination of the SiO_2 powder collected in this experiment using an XRD shows that it is amorphous in structure. Composition analysis by EDS indicates that the powder is composed of 99.6% SiO_2 and 0.4% SnO_2. In preparing samples for EDS analysis, the powder was fixed on the supporting aluminum blocks using glue containing silver . Since Ag and Sn have overlapped signals, the signal attributed to Sn may be from Ag. Further analysis is required to resolve this confusion.

Figure 3 shows three TEM micrographs of the powder. The powder can be divided into two types of particles. One is aggregates of very small particles, which are approximately 0.02 μm in diameter. The other is composed of larger, spherical particles whose diameters are approximately 0.1 μm. Some of these particles form aggregates (typically two to five together). However, some of them exist as

single particles. (It should be noted that single,spherical particles have not been found in the published studies on the formation of silica particles, using premixed flames [3,4].)

As illustrated in Fig. 4, we proposed a growth mechanism for the formation of the two types of silica particles in the counterflow diffusion flame. As the fuel gases flow out of the lower part of the burner, silane is oxidized to generate SiO_2 vapor. The SiO_2 vapor (in a supersaturated state) then nucleates and a large number of small particles are produced. These initially formed particles can grow by either vapor deposition or aggregation, or both. In the central part of the fuel gas stream, particles flow through the high-temperature flame zone. The previously formed aggregates fuse to form spherical particles as they pass through the flame zone. This process (as indicated by mechanism (a) in Fig. 4) may explain the formation of the larger, spherical particles found in this experiment. In the outer part of the fuel stream, particles do not pass through the high-temperature flame zone. The previously formed aggregates do not fuse to form spherical particles but remain as aggregates. Further formation of aggregates (or agglomerates) may occur due to interparticle collisions as the particles flow out of the burner. This process (as indicated by mechanism (b) in Fig. 4) may explain the formation of the aggregates of small particles found in this experiment.

B. Experiment Two

The TEM micrographs of the particles collected in this experiment show that all the particles are aggregates of small particles (approximately 0.02 μm in diameter) and that there is no larger, spherical particles. (see Fig. 5) Since silane was added to the side slots, particles may form by mechanism (b) as shown in Fig.4. (Therefore, all the particles are aggregates and no larger, spherical particles are formed.)

C. Experiment Three

The particles collected in this experiment also consist of two types of morphology as found in experiment one. However, there are more larger, spherical particles and less aggregates of small particles as compared with those obtained in experiment one. (See the TEM micrographs in Fig. 6) Since silane was added to the central slot, most particles may form by mechanism (a), thus leading to the formation of more larger, spherical particles. However, some particles in the outer part of the stream may form by mechanism (b), thus leading to the formation of aggregates.

CONCLUSION

Some conclusions may be drawn from the experiments described above: (1) high purity and submicron silica particles can be generated using the counterflow diffusion flame burner; (2) the original form of the burner produces two types of particles; (3) our modification of the burner offers the possibility for the control of the morphology of the particles; (4) the proposed mechanism seems to explain the formation of silica particles in the flame.

ACKNOWLEDGEMENT

Support of this research by the R.O.C. National Science Council is gratefully acknowledged.

REFERENCES

1. Shyan-Lung Chung and Joseph L. Katz, "The Counterflow Diffusion Flame Burner: A New Tool for the Study of the Nucleation of Refractory Compounds", Combustion and Flame, 61: 271 (1985).
2. Shyan-Lung Chung, "The Counterflow Diffusion Flame Burner: A New Tool for the Study of the Nucleation of Refractory Compounds", Ph.D. Dissertation, The Johns Hopkins University, Baltimore, Maryland, USA, 1985.
3. Ulrich, G.D., Riehl, J.W., "Aggregation and Growth of Submicron Oxide Particles in Flames," J. Colloid Interface Sci., 87, 257 (1982).
4. Ulrich, G.D., "Flame Synthesis of Fine Particles", Chemical and Engineering News, August 6, 1984, P. 22.

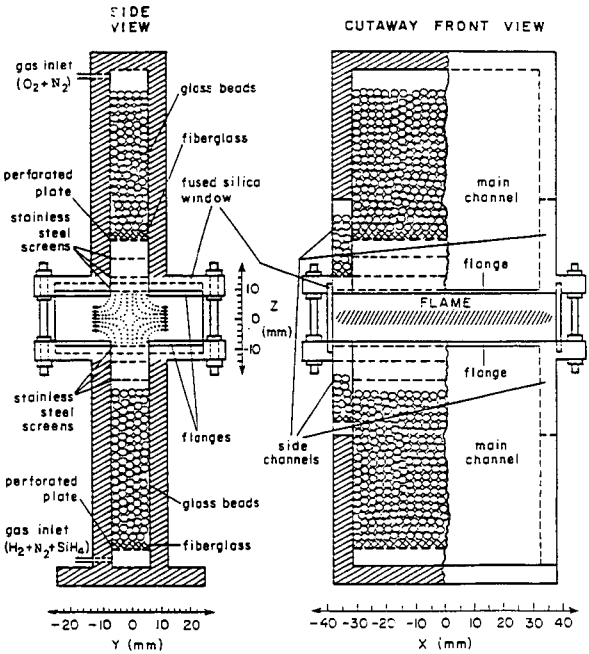

Fig. 1 The counter flow diffusion flame burner.

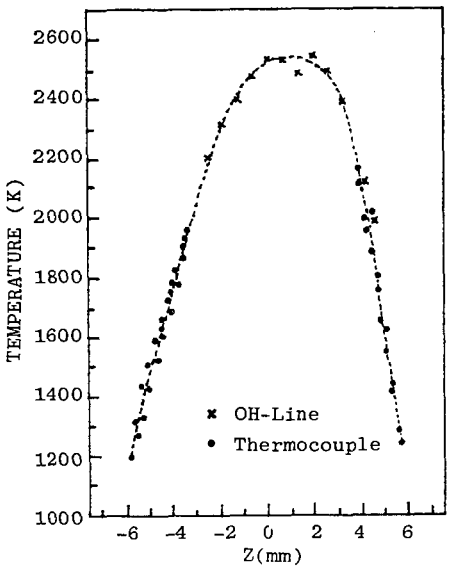

Fig. 2 Temperature distribution along the vertical direction in the counterflow diffusion flame.

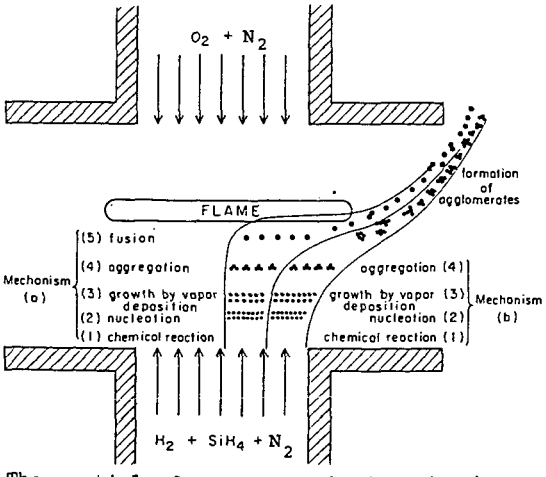

Fig. 4 The particle formation mechanisms in the counterflow diffusion flame.

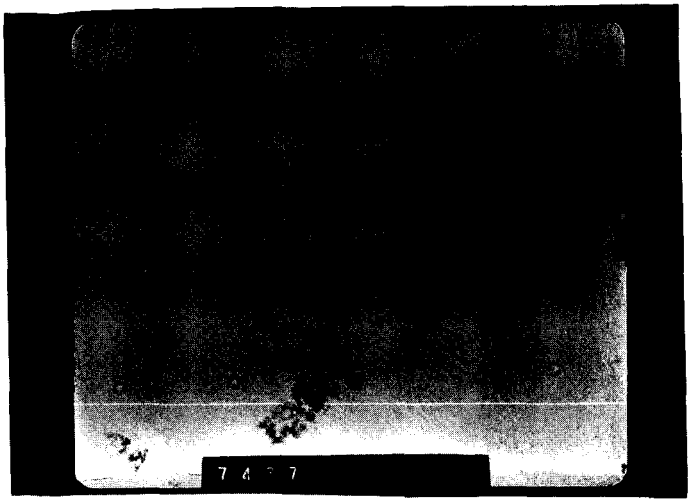

(a) 24,000×
(0.4 μm)

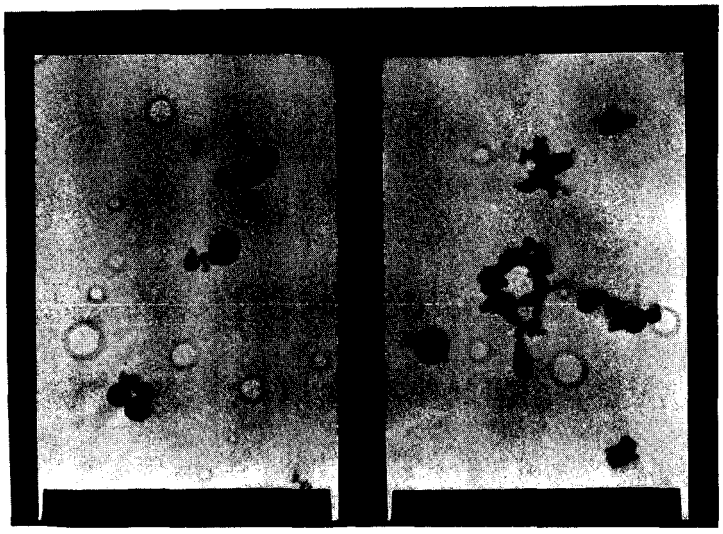

(b) 30,000×
(0.3 μm)

Fig. 3 TEM photographs of SiO_2 sample.

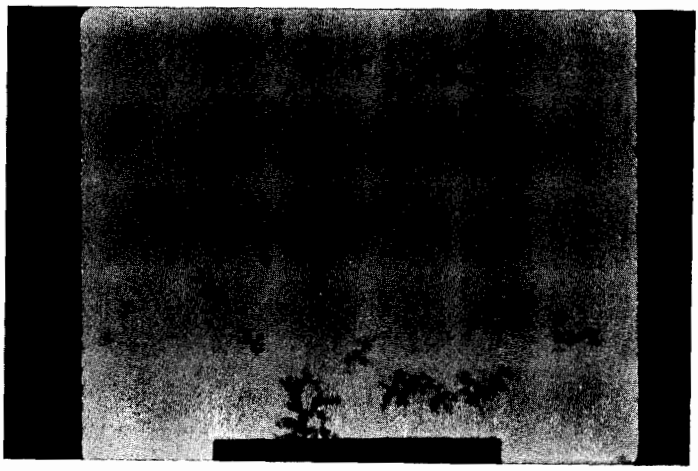

Fig. 5 TEM photograph of SiO_2 sample.
21,000× (0.4 μm)

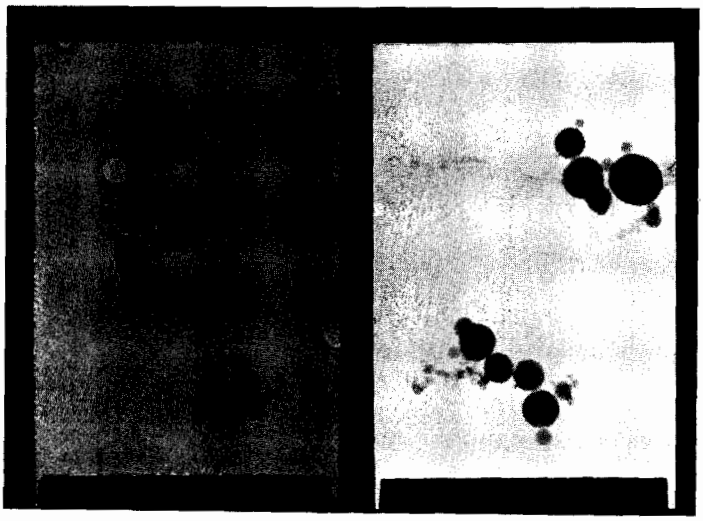

Fig. 6 TEM photographs of SiO_2 sample.
48,000× (0.2 μm)

EFFECT OF SEVERITY ON CATALYTIC HYDROPROCESSED SHALE OIL JET FUELS

N.L. MUKHERJEE

Chemical Engineering Department
Tuskegee University
Tuskegee, AL 36088

ABSTRACT

Catalytic hydroprocessed shale oil jet fuels in the USA were characterized and compared with petroleum jet fuel to demonstrate their possibility as a conventional jet fuel substitute. The shale oils (Geokinetics, Occidental, Paraho and Tosco II) were hydrotreated in a 0.0508m ID by K1.524m long reactor containing $Ni/Mo/Al_2O_3$ catalyst. The fractionated hydrogenated shale oils at jet fuel ranges (120-300^{0}C) were analyzed for composition and physical properties. The increasing hydroprocessing severity proportionally decreased nitrogen, sulfur, olefins, aromatics and increased hydrogen content. The nitrogen content was considerably higher even at high severity conditions. Sulfur and olefin contents were lower at all severities. The heat of combustion and the physical properties, except the freezing point, were comparable to petroleum jet fuels. The yields of jet fuels increased proportionally to increased severity. The study showed that high severity hydroprocessing gave better performance in processing shale oils to jet fuels.

INTRODUCTION

Shale oil jet fuels contain considerably higher nitrogen levels than petroleum jet fuels. These shale oil-derived jet fuels cannot be processed in a refinery similar to that used to obtain petroleum jet fuel because the high nitrogen content could poison the refinery catalyst. Nitrogen content greater than 5 ppm decreases fuel oil thermal stability and increases nitrogen oxide emissions during jet fuel combustion.

The present problem is to obtain a nitrogen level for jet fuel in the range of 1-5 ppm. High severity hydrodenitrification for the reduction of nitrogen content is not cost effective. The crude jet fuel cut can be chemically treated to lower the nitrogen level to an acceptable upper limit. Hydrogenation of shale oil fractions at low severity, prior to one of the chemical treatments [1] (acid washing, use of an hydrous acid, ion exchange resins, use of solvents, percolation over clays and acid absorbants, partial oxidation) has been shown to substantially lower the cost of producing jet fuel compared to severe catalytic hydrogenation. This hydrogenation operation also reduces the nitrogen level to an acceptable level (1-5 ppm). An increase of temperature [2] and pressure [3] proportionally increase the hydroprocessing severity, which facilitates the removal of nitrogen, sulfur and oxygen and the addition of hydrogen.

In the present work, shale oil hydroprocessing was performed at low, medium and high hydroprocesssing severities. The hydroprocessing severity was changed primarily by varying the temperature. Production

Table I Analysis of De-ashed/De-watered and Hydrogenated Shale Oil

Property	PARAHO				TOSCO II				GEOKINETICS				OCCIDENTAL			
	D-A/D-W	T_R=1.0	T_R=.92	T_R=.85	D-A/D-W	T_R=1.0	T_R=.92	T_R=.85	D-A/D-W	T_R=1.0	T_R=.92	T_R=.85	D-A/D-W	T_R=1.0	T_R=.92	T_R=.85
Hydrogen Content, Wt.%	11.74	14.00	13.46	12.92	11.23	13.80	13.20	12.34	12.28	13.72	13.31	12.85	12.31	13.60	13.20	12.81
Carbon Content, Wt.%	84.68	85.69	85.42	85.20	84.53	85.43	85.66	85.62	84.45	85.81	85.68	85.61	84.67	86.02	86.13	85.82
Nitrogen Content, Wt.%	2.08	0.19	0.90	1.60	2.15	0.60	0.90	1.61	1.71	0.33	0.74	1.20	1.53	0.25	0.40	1.05
Sulfur (Total), Wt.%	0.71	0.024	0.040	0.051	0.73	0.023	0.042	0.081	0.62	0.01	0.015	0.023	0.67	0.01	0.017	0.043
Density g/ml (60°C)	0.908	0.818	0.840	0.855	0.906	0.837	0.854	0.872	0.876	0.811	0.822	0.840	0.891	0.823	0.841	0.853
Pour Point, °C(°F)	21.2 (81)	23.3 (74)	23.9 (75)	23.3 (74)	20.6 (69)	19.4 (67)	19.4 (67)	21.1 (70)	12.8 (55)	25.0 (77)	23.3 (74)	16.1 (61)	12.2 (54)	23.3 (74)	4.4 (40)	6.1 (41)

of shale oil (Table I) hydroprocessing and distillation of the hydroprocessed product was carried out at NASA's Lewis Research Center bench-scale hydroprocessing facility. The process flow diagram (Figure 1) shows the jet fuel preparation from crude shale oil.

EXPERIMENTAL

De-ashed and de-watered shale oil containing 39% hydrocarbons (20% alkanes, 20% aromatics, 25% aromatic resins, 35% olefins and naphthenes) and 61% nonhydrocarbons (60% nitrogen, 10% sulfur and 30% oxygen compounds) was fractionated below 343°C. Shale oil fractions were hydrogenated in a reactor (length 1.524 m and diameter 0.0508m) containing American cynamide HDS-3A, Ni-Mo/Al_2O_3) catalyst of .025cm extrusions. The reactor contained four catalyst zones between non-reactive zones of Al_2O_3 extrusions of 0.3 cm diameter. Alumina zones equipped with wall heat-exchangers maintained nearly constant reaction temperature. The reactor's four catalyst zones were heated by four outside wall electric heaters and the hydrogen preheating (300°C) was accomplished by the electric heater at reactor top. The space velocity of the shale oil liquid in the reactor was 0.99-0.95 m^3/m^3 hr and the hydrogen comsumption was approximately 280 std. m^3/m^3 of shale oil. Shale oil fractions were hydrotreated at processing severities: (A) high=416°C and 1.413 x 10^4kpa (B) medium 382°C and 1.396 x 10^4kpa (C) low = 354°C and 1.327 x 10^4kpa. Figure 2 demonstrates hydrogen comsumption in shale oil at different processing severities. The hydroprocessed shale oil was fractionated (boiling range = 121-300°C) to produce jet fuel. Throughout the discussion, T_R is a temperature ratio indicating the severity of the run compared with high severity T_R=1.0-high severity, T_R=0.92-medium severity, T_R=0.85-low severity.

RESULTS AND DISCUSSIONS

Hydroprocessed shale oil jet fuels were distilled (ASTM D-86) at different boiling ranges (Figures 3, 4, and 5). The average boiling range of the high, medium and low severity hydroprocessed shale oil jet fuel cuts was 160-190°C for the 10 volume percent distillate and 260-270°C for the 90 volume percent distillate. Low and medium severity jet cuts have higher boiling ranges than high severity cuts because they contain more heavy hydrocarbons and heterocyclic compounds. The distillation temperatures and the volume percent recovery of the shale oil jet fuels are comparable to those of standard petroleum jet fuels (Table II). The results closely agree with the investigations of Shelton [4] who obtained a maximum boiling point of 195°C for 10 volume percent and 255°C for 90 volume percent recovery of a petroleum fuel.

Table II: Petroleum Jet Fuel Properties
(ASTM Methods)

Hydrogen content, wt%	16.00 max
Aromatics content, vol%	20 max
Nitrogen content (total), ppm	5 max
Sulfur content (mercaptan), wt%	0.003 max
Sulfur content (total), wt%	0.3 max
Naphthalenes contnt, vol%	3 max
Distillation temperature, °C	-
Initial boiling point	-
10 (vol%)	204 max

Table VII Analysis of Hydroprocessed Shale oil Jet Fuels.

PROPERTY	PARAHO			TOSCO II			GEOKINETICS			OCCIDENTAL		
	T_R=1.0	T_R=0.92	T_R=0.85	T_R=1.0	T_R=0.92	T_R=0.85	T_R=1.0	T_R=0.92	T_R=0.85	T_R=1.0	T_R=0.92	T_R=0.85
Hydrogen Content,wt%	13.85	13.53	13.33	13.78	13.50	13.14	13.68	13.64	13.29	13.78	13.64	13.45
Carbon Content,wt%	85.98	85.92	85.33	85.78	85.69	85.46	86.15	85.86	85.52	86.13	85.88	85.79
Nitrogen Content,wt%	0.122	0.418	1.16	0.366	0.655	1.16	0.140	0.428	1.06	0.038	0.355	0.725
Sulfur Content,wt%	<0.003	0.03	0.032	<0.003	0.022	0.039	<0.003	0.023	0.031	<0.003	0.021	0.025
Sulfur (Mercaptan),wt%	<0.0003	<0.0003	<0.0003	<0.0003	<0.0003	<0.0003	<0.0003	<0.0003	<0.0003	<0.0003	<0.0003	<0.0003
Aromatics Content,vol.%	19.0	19.7	19.9	22.4	22.5	23.1	19.4	22.0	22.8	20.1	22.7	23.7
Olefin Content, vol.%	0.6	3.2	4.5	1.1	1.5	3.3	1.1	1.7	2.8	1.0	2.1	2.6
Naphthalenes Content,vol.%	1.12	2.10	3.51	1.76	2.19	3.46	0.96	1.45	3.73	0.47	1.39	2.70
Flashpoint, °C (°F)	50.0 (122)	59.4 (139)	59.4 (139)	47.8 (118)	44.4 (112)	43.3 (110)	54.4 (130)	57.2 (135)	61.7 (143)	44.4 (112)	58.9 (138)	62.2 (144)
Specific Gravity, (15°C/15°C)	0.818	0.830	0.838	0.819	0.829	0.835	0.817	0.831	0.843	0.814	0.835	0.841
Freezing Point °C (°F)	-27.8 (-18)	-27.2 (-17)	-27.8 (-18)	-33.3 (-28)	-32.2 (-26)	-30.6 (-23)	-30.8 (-23.5)	-28.9 (-20)	-26.7 (-16)	-40.0 (-40)	-28.9 (-20)	-27.8 (-18)
Viscosity, $m^2/s(20^0C)$	$4.2x10^{-6}$	$4.7x10^{-6}$	$5.3x10^{-6}$	$3.5x10^{-6}$	$4.0x10^{-6}$	$5.1x10^{-6}$	$4.0x10^{-6}$	$4.5x10^{-6}$	$5.5x10^{-6}$	$2.3x10^{-6}$	$5.4x10^{-6}$	$5.7x10^{-6}$
Heat of Combustion kj/kg (Btu/lb)	42,282 (18,418)	42,998 (18,485)	42,374 (18,217)	42,549 (18,292)	42,530 (18,284)	42,246 (18,162)	43,072 (18,517)	42,356 (18,209)	42,428 (18240)	42,677 (18,347)	42,844 (18,419)	42,584 (18,307)

50 (vol%)	-
90 (vol%)	-
Final boiling point	300 max
Flashpoint, ^{0}C	38 max
Gravity (specific, 15/15^{0}C)	0.7753 to 0.8398
Freezing point, ^{0}C	-40
Viscosity at -20^{0}C, m^2/s	8×10^{-6} max
Net heat of combustion, kJ/kg (Btu/lb)	42,800 (18,400) min

Nitrogen content (Figure 6) in all severities is high in Tosco II and low in Occidental jet fuel. The amounts of Weak Base I and non-basic nitrogen compounds are variable in different types of shale oil jet fuels. High severity hydrotreatment significantly decreases [5] the nitrogen content of Weak Base I and non-basic nitrogen compounds, and Weak Base I can be removed more easily than non-basic nitrogen during hydroprocessing. High severity Occidental shale oil contains the lowest amount (0.03 wt%) of nitrogen of all shale oil jet fuels. This amount is significantly higher than that of petroleum jet fuel (1-5 ppm). The nitrogen content in low severity jet fuel is always higher than that of high severity jet fuel.

Table III shows the properties of shale oil jet fuels and also demonstrates that sulfur removal is proportional to severity. High severity jet fuels have the lowest sulfur content (0.003 wt%). Even the sulfur content in low severity jet fuels is lower than that of petroleum jet fuel (0.30 wt% maximum).

Increase of hydrogen content (Table III) in shale oil jet fuels is proportional to the severity of hydrotreatment. Severity increases saturation and cracking of hydrocarbons, thereby increasing the hydrogen/carbon ratio. Gunberger reported [6] the increase of hydrogen content from 11.40 wt% to 13.0 wt%. The hydrogen content (13-14 wt%) in shale oil jet fuel is relatively lower than that of standard petroleum jet fuel, which is 16 wt%. Aromatic content in shale jet fuels decreases with severity because of hydrocracking process. The effect of severity on aromatic content is the highest for Paraho, while Occidental shows the lowest. The aromatic content in shale oil jet fuels (except Paraho) is generally higher than in that of petroleum jet fuel, which is at maximum 20% by volume.

The freezing point of shale jet fuels is significantly higher than that of petroleum jet fuel (-40^{0}F) because shale jet fuels contain higher saturation fractions, particulary higher n-alkanes [7]. Freezing point decreases with increasing severity. Other physical properties such as flash point, viscosity, and specific gravity of the shale jet fuels decrease (Table III) with severity, and the values in all severities are within the acceptable limit of petroleum jet fuel specifications. Severity has little effect on heating values of shale jet fuels and the values are comparable to those of petroleum jet fuels.

CONCLUSION

1. High severity shale oil jet fuels constitute the hydrocarbons of more different boiling points than low and medium severity jet fuels. Aromatic and heavy hydrocarbon contents in low and medium severity are higher than in high severity jet fuels.

2. Increasing severity enhances nitrogen and sulfur removal. Nitrogen content is above, while sulfur content is much below, the acceptable limit of that of petroleum jet fuel.

3. Increasing severity increases hydrogen while it decreases aromatic content. Hydrogen content is a little lower while aromatic content is slightly higher than that of petroleum jet fuel.

4. Flash point, viscosity, and specific gravity decrease with increasing severity, and the levels in all severities are within acceptable limits. The freezing point is enhanced with increasing severity and is above the acceptable limit.

5. Increasing severity enhances yields of jet fuels. It can be concluded that high severity hydroprocessed Paraho jet fuel after processing can be considered as an alternative to conventional jet fuel.

REFERENCES

(1) Nowacki, P., Oil Shale Technical Data Handbook., Shale Oil Upgrading, Noyes Data Corporation, Park Ridge, New Jersey, 193 (1981).

(2) Cottingham, P.L., E.R. White and C.M. Frost, Hydrogenating Shale Oil to Catalytic Reforming Stock, Ind. Eng. Chem., Vol. 49, No. 4, 679-684 (1957).

(3) Frost, C.M. and P.L. Cottingham, Some Effects of Pressure on the Hydrocracking of Crude Shale Oil over Cobalt-Molybdate Catalyst, BM-PPRI-7835, Bureau of Mines (1974).

(4) Shelton, E.M., Aviation Turbine Fuels, U.S. Department of Energy, BETC/PPS-79/2 (1979).

(5) Holmes, S.A. and L.F. Thompson, Nitrogen-Type Distribution in Hydrotreated Shale Oils: Co-relation with Upgrading Process Conditions, 14th Oil Shale Symposium Proceedings, Colorado School of Mines Press, 242-243 (1981).

(6) Gunbeger, G.A. Logistics Management of Paraho Residual Shale Oil, Radian Corporation, Pasadena, CA, B-20 (1980).

(7) Newman, S.A., Shale Oil Upgrading and Refining Jet Fuel Freezing and Composition, Butterworth Publishers, Boston, 243 (1983).

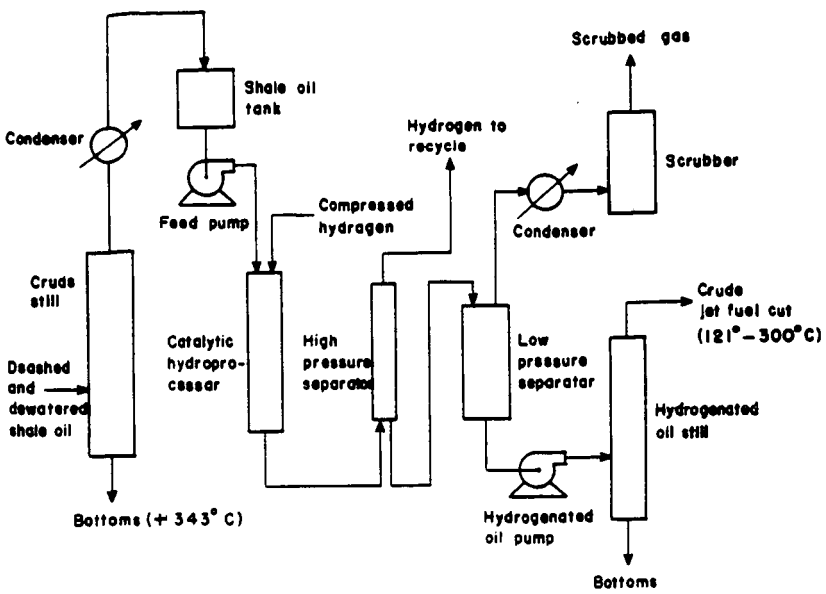

Figure 1. Process Flow Diagram to produce Shale Oil Jet Fuel

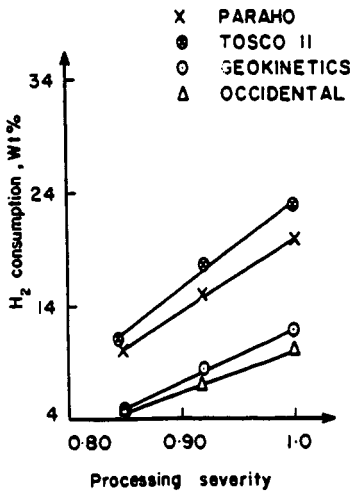

Figure 2. Hydrogen Consumption in Shale Oil Hydroprocessing

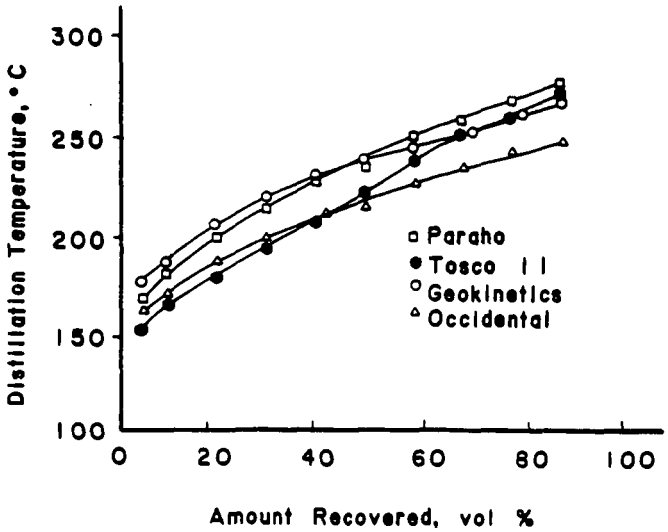

Figure 3. High severity Shale Oil Jet Fuel Distillation

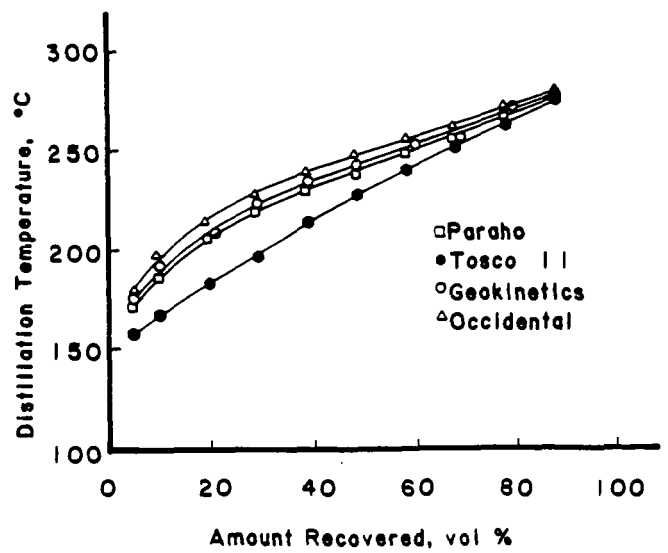

Figure 4. Medium severity Shale Oil Jet Fuel Distillation

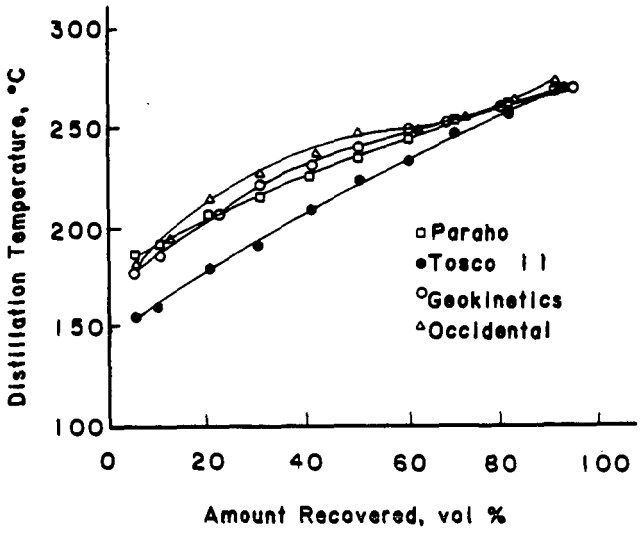

Figure 5. Low severity Shale Oil Jet Fuel Distillation

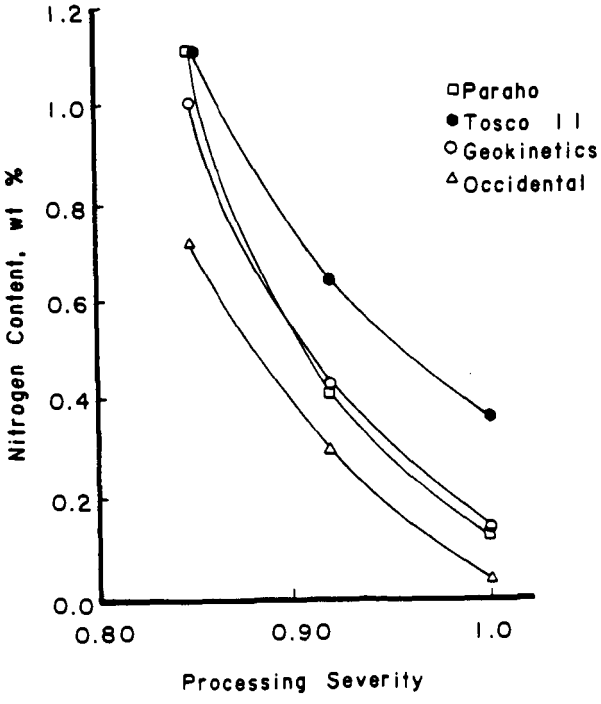

Figure 6. Nitrogen content in Shale Oil Jet Fuel